ABSTRACT

Title of Document:	NANO ELECTRIC DISCHARGE MACHINING OF GOLD THIN FILMS WITH A MODIFIED SCANNING TUNNELING MICROSCOPE.
	Marcia A. Golub, Master of Science, 2005
Directed By:	Professor Romel D. Gomez, Department of Electrical and Computer Engineering

This Master's thesis presents the development of an instrument and a technique to locally ablate solid surfaces using a scanning tunneling microscope and an electrostatic discharge processes. The design and construction of the scanning tunneling microscope inside the scanning electron microscope along with the designs of the control electronics are reported. Several methods of surface modification are investigated, namely mechanical contact and near-surface discharge in air and vacuum. Images of gold and graphite surfaces in air and vacuum, and feature formation using electrostatic discharge in air and vacuum are discussed. Analysis of the relationship between energy of the discharge and feature's size is presented, along with a discussion of the geometrical characteristics of the features.

NANO ELECTRIC DISCHARGE MACHINING OF GOLD THIN FILMS WITH A MODIFIED SCANNING TUNNELING MICROSCOPE.

By

Marcia A. Golub

Thesis submitted to the Faculty of the Graduate School of the
University of Maryland, College Park, in partial fulfillment
of the requirements for the degree of
Master of Science
2005

Advisory Committee:
Professor Romel D. Gomez, Chair
Professor John Melngailis
Professor Lourdes G. Salamanca-Riba

Dedication

To my parents and my grandparents,

for their love and support.

Acknowledgements

Though many solitary hours are spent working on an experiment, one can never truly complete a project alone. Accordingly, I extend my gratitude to Prof. R.D. Gomez, who advised me throughout this project and designed the original layout of the STM. Also, I would like to thank J.B. Dottellis and Les Lorenz for machining the STM parts and the inertial motor, and Konrad Aschenbach for his help with circuits.

I would particularly like to thank Dr. Michael Dreyer for designing most of the circuits, providing insightful suggestions and helping me at every step of the way. His altruism and dedication to science is the backbone of our group.

Finally, I wish to thank all the group members: Sylvia Florez, Herman Pandana, Jookyung Lee, and Ronald De Los Reyes for their continuous support and for sharing their expertise in various areas.

Table of Contents

List of Tables

List of Figures

Introduction

In the age of electronics governed by Moor's law it is becoming more and more important to be able to create preconceived structures on solid surfaces on nanometer scales. A crucial first step towards this end is the development of a technique for direct and highly controlled material removal. Combining a scanning tunneling microscope (STM) and an electric discharge machining (EDM) is an ideal approach to achieve this goal. The STM's capability for atomic imaging and positioning control can be used in conjunction with the effective material removal rate of the EDM process.

In this experiment, I successfully built a scanning tunneling microscope inside a scanning electron microscope, and obtained images of gold and graphite (HOPG) surfaces in air and in vacuum. I also built the circuitry necessary to control the STM/NanoEDM system and produced sub-micron surface modifications on thin Au films by means of mechanical contact and electrostatic discharge in air and in vacuum. I investigated the phenomenon responsible for creating small features, and established a correlation between features' size and shape and the conditions under which they were produced.

The experimental setup consists of three major instruments that are integrated to work together. The three major instruments are Scanning Electron Microscope (SEM), Scanning Tunneling Microscope (STM) and Electric Discharge Machine (EDM). The combination of these instruments creates a new system, which is called Nano-Electrіc Discharge Machine (NanoEDM). The principles of operation of these instruments as well as their significance in this experiment are going to be discussed

in the following chapters.

Chapter one describes electric discharge machining that is commonly used in industrial applications to machine delicate parts. It gives a detailed overview of the principle of operation of EDM, its parameters, discharge related theory and theoretical and empirically established formulas.

Chapter two gives an overview of scanning tunneling microscopy and the theory behind it; and describes in detail different parts of an STM, such as piezo scanner, inchworm motor and STM tips. Chapter three gives an overview of scanning electron microscopy. It describes the principles of operation of the SEM and different types of electrons that can be monitored to give full information about the sample.

Chapter four gives a complete description of the experimental set up, including all the parts that were designed and built specifically for this project, as well as instruments that are commercially available. It gives a step by step description of procedures used to modify the surface and the procedure for making electro-chemically etched tungsten tips.

Chapter five describes the results produced during the experiments. It shows images of surface modifications produced by different methods and under different conditions. It also gives tables of experimentally obtained values and graphs of the given data.

Appendices offer a complete description of the blue prints that were used to build the experimental setup, such as AutoCAD drawings of STM parts, layout of the circuits, and tables that list all the connection pins between the STM and EDM circuitry.

Chapter 1: Electric Discharge Machining (EDM)

1.1 Overview

Material removal by an electric spark was first studied in the early 1940's by two Russian scientists B.R. and N.I. Lazarenko, who were investigating the erosion of electrodes when a voltage was applied between them. At the same time three Americans, H.L. Stark, H.V. Harding and J. Beaver were developing a new technique to remove broken taps from hydraulic valve bodies. The result of these studies was the prototype of the modern day EDM [1].

EDM is a type of surface modification classified under nontraditional machining processes. Other non-conventional machining methods include such diverse areas as mechanical, chemical, electrical, laser beam, and water jet machining techniques. A complete classification can be seen in figure 1.1.

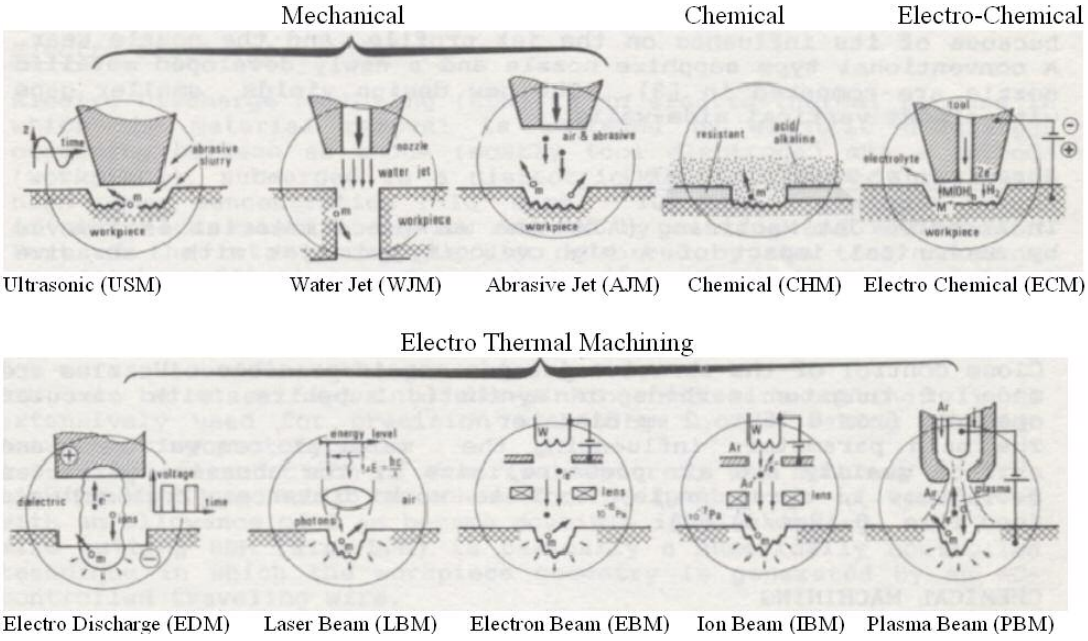

Figure 1.1 Classification of non-conventional machining methods, based on appearance of energy [2]

EDM is an electro-thermal process; it converts electrical energy into thermal energy that is used to remove the material. Nontraditional machining is used when the traditional machining methods such as chip formation and abrasion are not satisfactory in producing a part with the desired requirements. The following reasons can be given to consider using a nontraditional method [3]:

a) The hardness and strength of material is above 400 HB or the material is too brittle
b) The workpiece is too delicate to withstand traditional cutting and grinding forces
c) The shape is complex and includes internal and external profiles or small holes
d) Surface finish and dimensional tolerance requirements cannot be achieve by standard methods
e) Temperature rise and residual stress in the workpiece are not acceptable

Most of the above reasons are applicable for choosing the EDM process: since the direct contact with the workpiece does not take place, the material of any hardness or softness can be machined as long as it is conductive. Both metals and semiconductors can be used in this process. Delicate parts can be hardened prior to being machined in order to avoid any damage. Different types of EDM are available for machining complicated designs: special rotating electrodes can be used to create internal cavities, wire EDM works like a saw to cut through the material, and die-sinking EDM is used for creating imprints on the surface that are mirror opposites of the electrode (die). Due to the nature of the process the material removed per cycle is miniscule; this provides great control over the surface finish and high precision in dimensional tolerance. Even though thousands of cycles can occur per minute, EDM

should not be used to machine a piece from scratch. It should rather be used to create the desirable surface parameters after the bulk of the material has been removed by conventional machining methods. Also EDM should not be used if the material is heat sensitive, since colossal temperature changes occur during each cycle, when the affected area of the workpiece melts and solidifies in a matter of microseconds. This solidification creates large tensile residual stress on the surface of the material, which may result in micro-crack formation on the surface.

1.2 Principles of Operation of EDM

The material removal in EDM occurs when an electrode and a workpiece are brought closely together and a voltage applied between them produces a spark. The electrode and the workpiece are submerged in a dielectric fluid and a constant separation is maintained between them. The discharge occurs when the voltage is high enough for the dielectric fluid to become ionized and thereby provide a path for the electrical current to flow. A small area of the workpiece affected by the discharge becomes sufficiently hot for the material to melt and for the dielectric fluid to vaporize. Small amounts of the melted material (about 10% [4]) fuse together into small particles that are flushed away by the dielectric fluid. The rest of the melted material resolidifies on the surface of the workpiece forming a “recast layer” between 1 and 30 micrometres thick [4]. The process is then repeated many times until the cavity formed on the surface of the workpiece is a mirror image of the electrode. This allows for the creation of any desired shaped on the surface of the workpiece and is known as die-sinking EDM. Figure 1.2 on the next page illustrates basic die-sinking EDM set up.

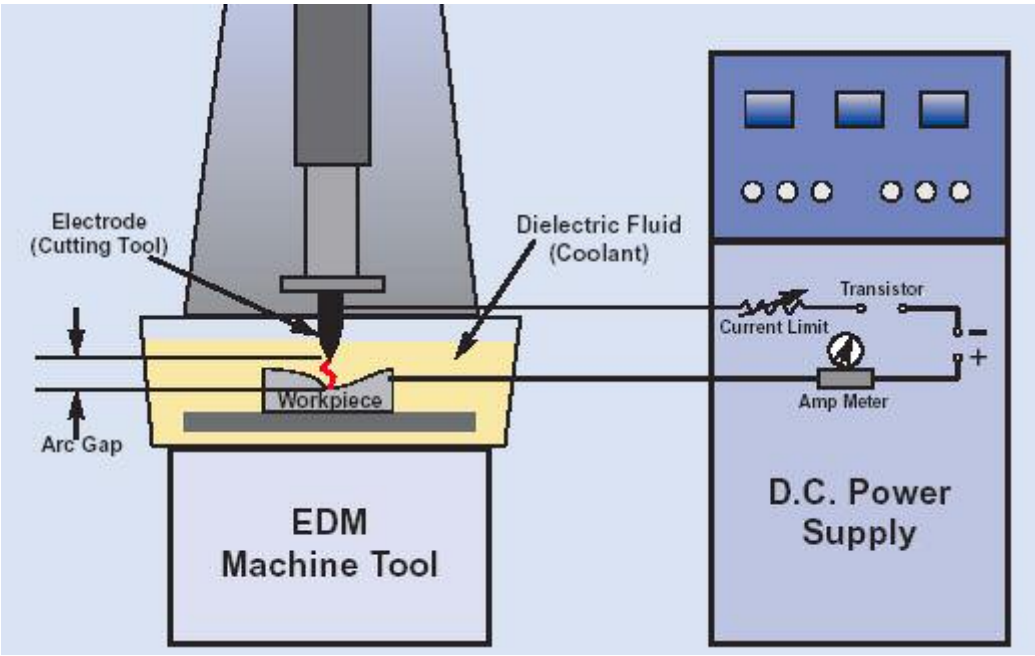

Figure 1.2 The electric discharge machine. The electrode and workpiece are held by the machine tool (left), which also contains the dielectric system. The power supply (right) controls the electrical discharges and the movement of the electrode in relation to the workpiece. [5]

The electrode is affected by the discharge in a similar way that the workpiece is affected by it. Although the material removal rate for electrode is smaller than it is for the workpiece, the electrode is also eroded by the process and the gap between the workpiece and the electrode over time becomes large enough to prevent the discharge from taking place. To avoid this problem the gap distance has to be monitored continuously during the machining process and the position of the electrode has to be adjusted to maintain a constant gap. This is a painstaking process to be done manually and therefore a servo control mechanism is employed to control the position the electrode. Modern EDM processes have become completely automated, requiring little interference from the operator after the process parameters, such as applied voltage, discharge current, and on-time, have been set.

1.3 Discharge Energy

The energy produced during the discharge or the power of the discharge can be described by equation 1.1 [1]

$$E = \frac{1}{2}UIt \tag{1.1}$$

where E is power of the discharge, U is the gap voltage during the discharge, I is current flowing during the discharge, and t is the length of time that the current flows. It is important to differentiate U and V, where V is the voltage applied to the workpiece before the discharge occurs. During the discharge the voltage V drops down to a fraction of the original value. The resistance between the electrode and the workpiece breaks down during the discharge and since the current is kept constant by the power supply, the discharge voltage has to go down according to Ohm's law (U=IR). The discharge voltage in this case is independent of the current and is dependent on the resistance of the gap, which is determined by the dielectric, and workpiece and electrode materials.

The discharge energy can also be determined by the capacitor used in the power supply circuit. The capacitance value can be expressed in terms of gap current I, discharge voltage U, and length of discharge t (eq. 1.2) [1].

$$C = \frac{It}{U} \tag{1.2}$$

The discharge energy can be rewritten in terms of capacitance C (eq. 1.3) [1].

$$E = \frac{1}{2}CU^2 \tag{1.3}$$

1.4 Discharge Process (Superheating Theory)

A closer examination of what happens at the moment of discharge reveals that a plasma channel is formed between the electrode and the workpiece when the dielectric breakdown occurs and the current begins to flow. In other words, the dielectric fluid is ionized and electrons and ions begin to flow to anode and cathode respectively. A gas bubble is formed by vaporized dielectric fluid, surrounded by a layer of compressed liquid. The ambient dielectric fluid surrounding the gas bubble pushes back on it, preventing the plasma channel from expanding. This causes the input energy (eq 1.1) to be concentrated in a very small volume, which heats up the plasma to very high temperatures on the order of 10^4 K [6]. The plasma channel is illustrated schematically in figure 1.3.

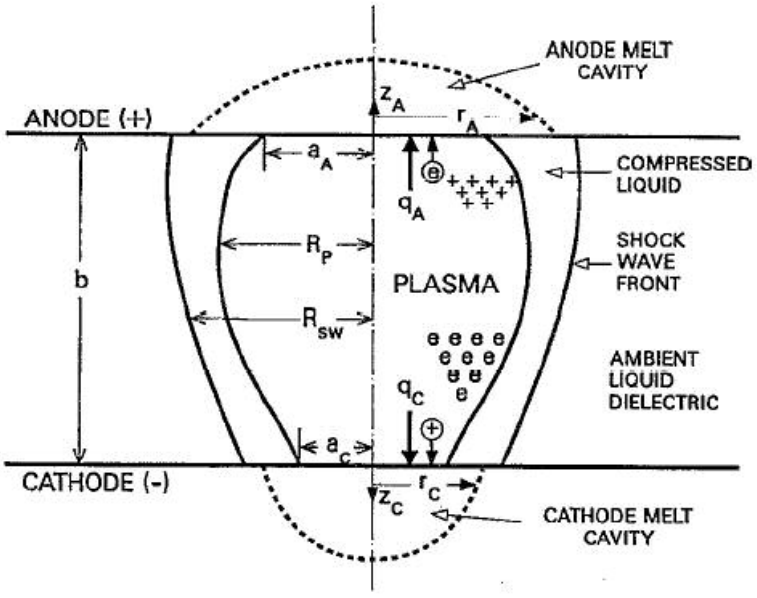

Figure 1.3 A schematic diagram of the EDM process showing plasma configuration and melt cavities in both electrodes [6].

The input energy in the form of heat is divided into three parts, the main part, about 74%, goes into the plasma formation and is absorbed by the dielectric fluid at the end of the discharge; 18% of the energy goes to the cathode, which in most cases

is the workpiece, and the remaining 8% of heat is absorbed by the anode (electrode) [7]. A Gaussian heat input model can be used to approximate the heat transferred to the workpiece and is given in equation 1.4 [8]

$$q(r) = FUI \exp\left(-\frac{r^2}{a^2}\right) \qquad (1.4)$$
$$a \propto t^{3/4}$$

where *q(r)* is the heat energy transferred to the workpiece, *F* is the fraction of the total energy conducted to the workpiece, *r* is the radial distance at any point from the central axis of the plasma and *a* is the plasma radius at the cathode. The plasma radius varies with time *t* measured in ms and *a* is measured in µm. *U* and *I* are voltage and current respectively as defined previously for equation 1.1. Since the percentage of energy that goes to the cathode was determined to be 18% byEubank et al [7] equation 1.4 can be rewritten as follows (eq. 1.5)

$$q(r) = 0.18UI \exp\left(-\frac{r^2}{t^{3/2}}\right) \qquad (1.5)$$

The diffusion of heat through the workpiece can be represented by equation 1.6.

$$\frac{\partial \tau}{\partial t} = D_\tau \nabla^2 \tau$$
$$D_\tau \equiv \frac{K}{\hat{C}} \qquad (1.6)$$
$$\hat{C} = \frac{\partial \rho_u}{\partial \tau}$$

where τ is temperature, D_τ is thermal diffusivity, *K* is the thermal conductivity of the workpiece, $\hat{C}$ is the heat capacity per unit volume and ρ_u is energy density.

The high temperature inside the gas bubble causes the electrode and the workpiece to melt. The metal actually reaches the vaporization temperature, but the

material does not vaporize due to the high pressure inside the plasma. The anode melts first but then solidifies after a few microseconds followed by the melting of cathode. The maximum cathode erosion occurs at about 30 µs, whereas the maximum anode erosion occurs at 3 µs as can be seen in figure 1.4. Therefore to achieve a lower tool to workpiece wear ratio the on-time for the spark should be 10 to 100 µs long. The graph in figure 1.4 is obtained from experimental data by DiBitonto et al for a copper anode and steel cathode and discharge current of 10 Amp.

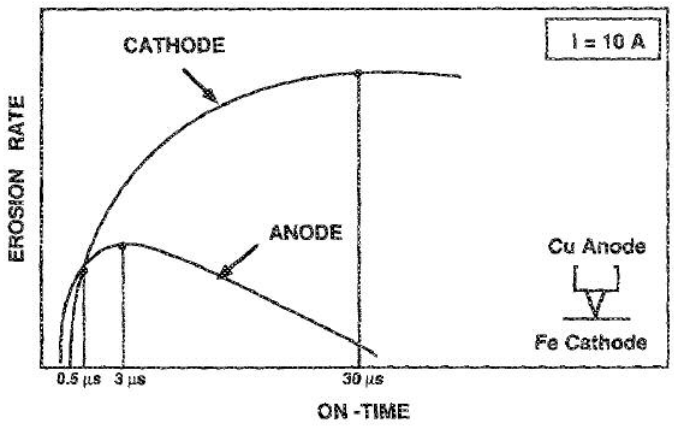

Figure 1.4 Anode and cathode erosion rates [6]

The anode melts first because the electrons in the plasma channel move faster than the ions and therefore the anode reaches the melting temperature before the cathode does. The plasma radius at the anode is larger than it is at the cathode thus the input heat is distributed over a larger area, and therefore melted material solidifies faster at the anode. This is consistent with the heat input model of equation 1.4 where *q(r)* is exponentially dependent on the inverse of plasma radius. The difference in plasma radius between the anode and the cathode is attributed to the fact that when the dielectric fluid is ionized the electrons are concentrated near cathode and the ions are concentrated near the anode. Since the electrons are much smaller in diameter

than ions the plasma radius is larger at the anode.

Due to the high pressure inside the plasma channel the molten metal on the surface of the cathode is held in place and no vaporization occurs. Trying to escape the high pressure inside the plasma channel the metal is pushed away from the center of the channel and concentrates around the edges, where it begins to solidify [8]. This phenomenon is responsible for creating crater walls around the indentation on the surface of the workpiece. When the supplied voltage is turned off the plasma channel and the gas bubble collapse violently and dielectric fluid rushes in. The change in pressure causes the molten metal on the surface of the workpiece to explode and solidify on contact with the cooler dielectric fluid. Small metal particles created during the explosion are flushed away by the dielectric fluid and the rest of the material solidifies on the surface. A small crater is created on the surface of the workpiece at the end of the discharge. An SEM image of such craters can be seen in figure 1.5.

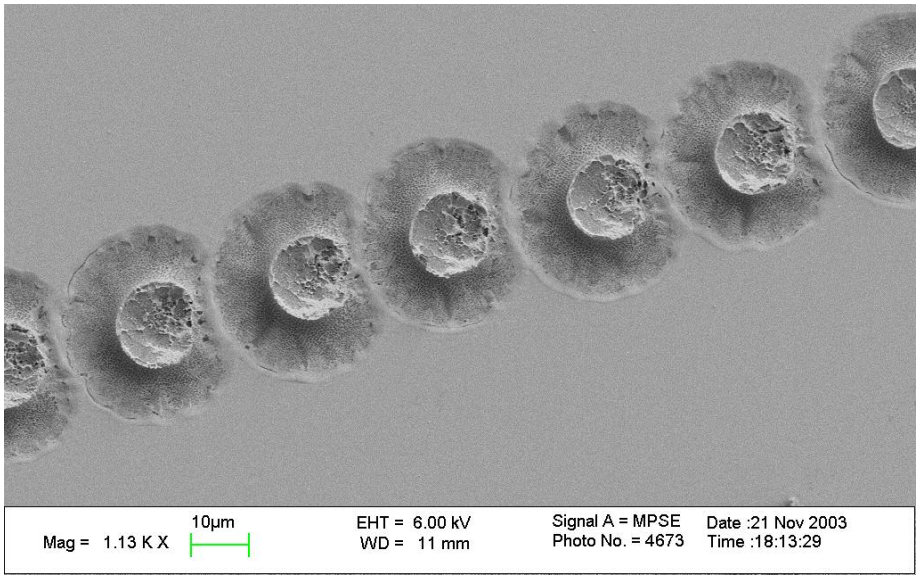

Figure 1.5 SEM image of craters created during EDM discharge

1.5 Material Removal Rate

The metal removal rate in the EDM process depends largely on the amount of energy produced during the discharge, which is turn depends on the capacitance of the discharge control circuit (eq. 1.3); it also depends on the amount of metal removed during one discharge and the frequency of discharges. Melting point also determines the rate of material removal, the lower the melting point of the workpiece the higher the removal rate. The equations 1.7 and 1.8 have been established empirically [1].

$$R_w = 2.43 M_w^{-1.23} \tag{1.7}$$

$$V_R = 1.36 \times 10^{-4} M_w^{-1.43} \tag{1.8}$$

Where R_w is the average metal removal rate from a workpiece measured in in^3/Amp-min.x10^4, M_w is the melting point of the workpiece in °C, and V_R is the average volume removed per discharge in in^3.

1.6 Electrodes and Electrode Wear

The electrodes are usually made out of graphite, but can also be made out of tungsten alloys, copper or other materials with a high melting point. A quantity that is important to consider is the electrode wear, since during the discharge the energy produced affects both the workpiece and the electrode. Electrode wear is inversely related to the melting point of the material used as the electrode, the higher the melting point the lower the wear. Therefore a high melting point of the electrode is critical in minimizing the tool wear. It is important to make electrodes out of materials that are difficult to melt; at the same time the material used as an electrode

should be relatively easy to machine, allowing for easy manufacturing of complex shapes.

Graphite is commonly used to make electrodes since it has an important property of being able to vaporize without melting. The energy required to vaporize a given volume of material is much larger that the energy required to melt the same amount of material, thus graphite has a low electrode-to-workpiece wear ratio. Two equations have been established empirically to calculate the electrode wear (eq. 1.9 and eq. 1.10) [1].

$$R_t = 6.51 \times 10^2 M_T^{-2.28} \quad (1.9)$$

$$W_R = 2.25 M_R^{-2.3} \quad (1.10)$$

Where R_t is the average metal removal rate from electrode measured in in^3/Amp.-min.x10^4, M_T is the melting point of electrode in °C, W_R is the workpiece to electrode wear ration, and M_R is the melting point ratio of workpiece to electrode.

1.7 Dielectric Fluid

The purpose of the dielectric fluid is threefold, it provides non-conductive barrier between the electrode and the workpiece, it removes the debris created during the discharge, and it cools the electrode and the workpiece. Clear fluids with low viscosity are used for this purpose. Hydrocarbon oils are commonly used as dielectric fluid; deionized water can also be used for EDM micro-hole drilling and kerosene can be used with tungsten electrodes. Some of the desirable characteristics for a dielectric fluid are low viscosity, high dielectric strength, and high flash point.

1.8 Parameters Commonly Used

The voltage (V) used in EDM range from 50 to 400 V, the current ranges from 0.1 to 500 A. The frequency of discharge is between 50 and 500 kHz with the arc time lasting between 10^{-7} to 10^{-2} seconds. The material removal rate in EDM ranges from 2 to 400 mm^3/min, with the amount of material removed per discharge ranging between 10^{-6} to 10^{-4} mm^3. Typical gap between the electrode and the workpiece is in the range of 10 to 100 micrometres. [1]

Chapter 2: Scanning Tunneling Microscopy (STM)

Scanning tunneling microscopy provides a convenient and easy way to obtain a three dimensional image of a surface on a nanometer or even atomic scale. Soon after its invention, the STM found applications in many diverse fields such as material science, semiconductor physics, and biochemistry. STM's main advantage is the ability to image the surface without damaging it by physical contact. Another advantage is that it is able to operate at ambient pressure, eliminating the need for high vacuum systems.

2.1 Historical Background

The prototype of the modern day scanning tunneling microscope was invented by an American physicist Russel Young. He was the first one to realize the advantage of scanning the tip very close to the surface without actually touching the sample. He designed a system that operated on a principle of field emission and was able to maintain a gap distance of 200 Å. However, this microscope was not able to produce a desirable resolution. Young realized that to improve the microscopes performance he would have to scan at much closer distances of about 10 Å, where electron-tunneling effect could occur even at low voltages. Unfortunately due to experimental difficulties he was not able to implement his idea.

First successful scanning tunneling microscope was built in 1981 by IBM researchers, Gerd Binnig and Heinrich Rohrer, at the Switzerland laboratory. They solved the vibration isolation problem by placing the microscope on large permanent magnet floating in a pool of superconducting lead. This helped eliminate the noise

associated with floor vibrations and they were able to resolve individual atoms in their images. For their work they received the 1986 Nobel Prize in Physics. [9]

2.2 Principle of Operation

The main component of the STM is a scanner, shaped as a tube and made out of piezoelectric material. The scanner allows the tip and the surface of the sample to approach very closely without physically touching each other. The tip and the sample are held at a given potential. When the tip is within tunneling range from the sample a current begins to flow between them. By monitoring the current the vertical position of the tip can be adjusted to maintain a constant gap between the tip and the sample as the tip scans over the sample. The data obtained from the tip's position is used to reconstruct the topographic image of the surface. Schematic structure of the STM is illustrated in figure 2.1.

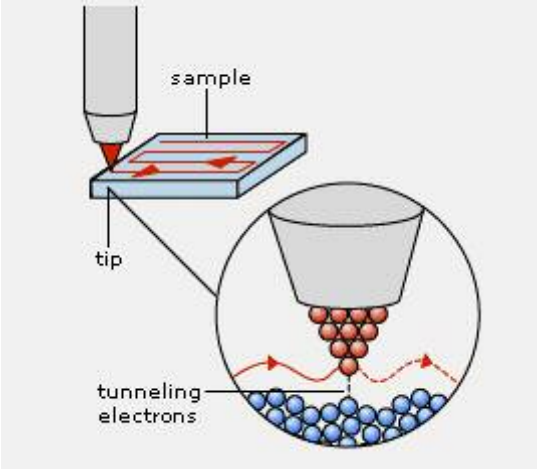

Figure 2.1 Schematic representation of the STM's principle of operation [10]

One of the advantages of the STM that allow it to obtain atomic resolution is the exponential dependence of the tunneling current on the distance between the tip and the sample (eq. 2.1) Based on this equation, even small changes in distance

produce large changes in tunneling current, allowing for the proper positioning of the tip and obtaining an atomic resolution of the sample.

$$I \propto e^{-2\kappa z} \tag{2.1}$$

Where I is the tunneling current, z is the tunneling gap, and κ is defined by equation 2.2.

$$\kappa = \frac{\sqrt{2m(V-E)}}{\hbar} \tag{2.2}$$

Where m is the mass of an electron, $\hbar$ is Plank's constant, E is the energy of the electron, and V is the potential in the gap. The average work-function of the tip and the sample is $\Phi = V\text{-}E$. Equation 2.1 can be rewritten as equation 2.3 to give a better approximation for the tunneling current.

$$I = C\rho_t\rho_s e^{-z\sqrt{k}} \tag{2.3}$$

Where ρ_t is the electron density of the tip, ρ_s is the electron density of the sample, C is a constant, and k is a wave vector. [11]

2.3 STM Tips

The tips used in STM are usually metal wires that have been sharpened on one end by electrochemical etching or mechanical cutting. Ideally the tip should be sharp enough that only one atom forms the pinnacle of the tip. The finer the tip the better the resolution that can be obtained. Common materials used to make the tips are Platinum-Iridium (Pt-Ir) and Tungsten (W) wires. The advantage of using tungsten tips is that they are more robust than Pt-Ir tips and can be made sharper, but the disadvantage is that they oxidize in ambient environment. Therefore Pt-Ir tips are used if the STM is operated in air and tungsten tips if it is in vacuum.

2.4 Scanner

The piezo tube scanner is used to precisely position the tip within tunneling range of the sample's surface and to scan the tip over the sample. The piezo tube is made out a piezoelectric material (polarized ceramic) that changes shape when a voltage is applied across it. Piezoelectric material can elongate or contract when the voltage is applied across it, depending on the polarity of the voltage. The inside and the outside walls of the tube are covered with thin metal layers that serve as electrodes. The metal layer on the outside of the tube is first sectioned horizontally creating top and bottom part; the top part is then sectioned vertically into four equal parts. The inside layer is sectioned in the same way. As a result the bottom part of the tube controls the vertical motion of the tip, while the top part controls the lateral motion. When a positive voltage is applied across the bottom part of the tube the piezo extends and the tip moves forward. To move the tip in the lateral direction the voltage of opposite polarity is applied to the two top sections that are facing each other. This causes one section to contract and the other section to extend, causing the tip to move sideways.

An important characteristic of a piezo tube is its scan range, which is determined by the piezoelectric constant of the material, the size of the tube, and the maximum voltage that can be applied before the piezo element depolarizes. Larger scan ranges come at the expense of reduced resolution. Longer piezo tubes introduce more instability and vibration to the system due to their higher dependence on the electrical noise of the high voltage power supply. Higher sensitivity to the electrical noise is translated to the mechanical noise of the scanner.

The other important parameter used to characterize scanners is resonance frequency, which should be relatively high. If the scanning frequency of the STM is comparable to or larger than the resonance frequency of the piezo tube, the scanner will not respond properly to the electrical signals. Therefore it is only possible to scan at frequencies that are lower than the resonance frequency of the scanner. The resonance frequency of the piezo tube depends on the length and the thickness of the tube and on the Young's modulus of the material. The Young's modulus in this case is used to estimate the equivalent spring constant of the tube. The resonance frequency also depends on the density of the piezoelectric material, since the density determines the inertial mass of the system.

2.5 Inchworm Motor

While the scanner takes care of approaching the surface within 10 Å, a mechanism with a more extensive range is needed to bring the tip within a few micrometers of the surface. The motor used for that purpose in our case is a piezo-electric device called the inchworm. The inchworm has a driving range of several centimetres with a step size of only 20 Å. Its main component is a piezo element that expands and contracts when the voltage is applied to it to move the tip closer to the surface. The diagram of motion of the inchworm and the corresponding inchworm drive signals are shown in figure 2.2.

The inchworm consists of two piezo clamps connected by a long piezo element. The clamps are positioned around a load-bearing rod. One of the clamps is attached to the body of the motor and is stationary, while the other clamp is not attached and can move along the rod. The inchworm moves according to the

following sequence. Voltage is first applied to clamp 3, this holds down the rod at the right end. The voltage is then applied to the piezo element and it extends to the left. At this point clamp 1 is activated and after that clamp 3 is released. The voltage is then turned off from the piezo element, which causes it to contract, subsequently moving the rod to the right. Interchanging clamp 1 and clamp 3 in the step sequence will result in the inchworm moving the rod to the left.

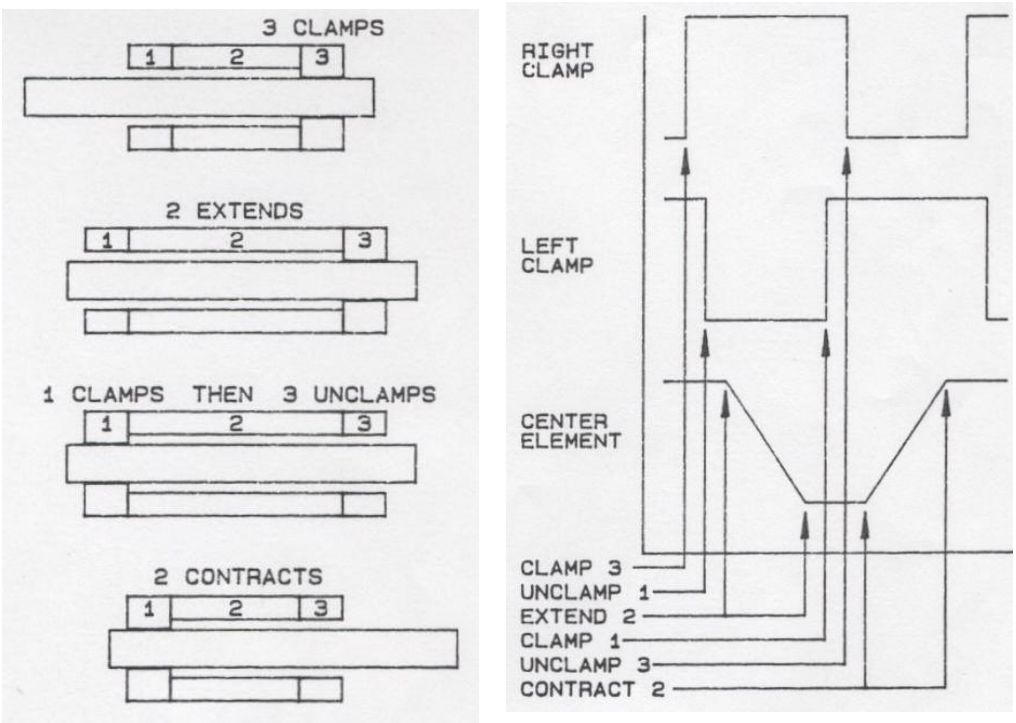

Figure 2.2 Inchworm motion diagram and corresponding inchworm drive signals [12]

Chapter 3: Scanning Electron Microscopy

3.1 Overview

The scanning electron microscope was invented as an innovative approach to overcoming the limitations of optical microscopy. All optical microscopes, no matter how well they are built and how perfect their lens may be, have one intrinsic limitation: they cannot resolve features that are smaller than half the wavelength of light. This means that if the object is smaller than ~0.25 µm it cannot be seen with an optical microscope.

To solve this problem the German physicist Ernst Ruska came up with a microscope that used electrons instead of photons to image objects, since electrons have a much shorter wavelength than photons. He realized that a magnetic coil could act as a lens to focus electrons in a similar way that a glass lens is used to focus light. Using this principle and coupling several magnetic lenses in a similar way that the optical microscope is constructed he was able to build the first electron microscope in 1933. In recognition of his invention he was awarded half of the 1986 Nobel Prize in Physics, which he shared with the inventors of the STM. The invention of the SEM allowed scientists to see features on a nanometre scale, making the SEM one of the most important inventions of the 20th century. [9]

3.2 Principle of Operation

The design of a modern day SEM is shown if figure 3.1. It is critical that the SEM is operated in vacuum, since the electrons are charged particles and can easily interact with the other electrons in air. The SEM operates by focusing a beam of

electrons on the surface of the sample, and then scanning the beam over the sample in a similar way that the tip is scanning the surface in STM. Electrons are then collected in a detector to form the image. If the air were to be present in the SEM chamber the information collected by the detector would be distorted.

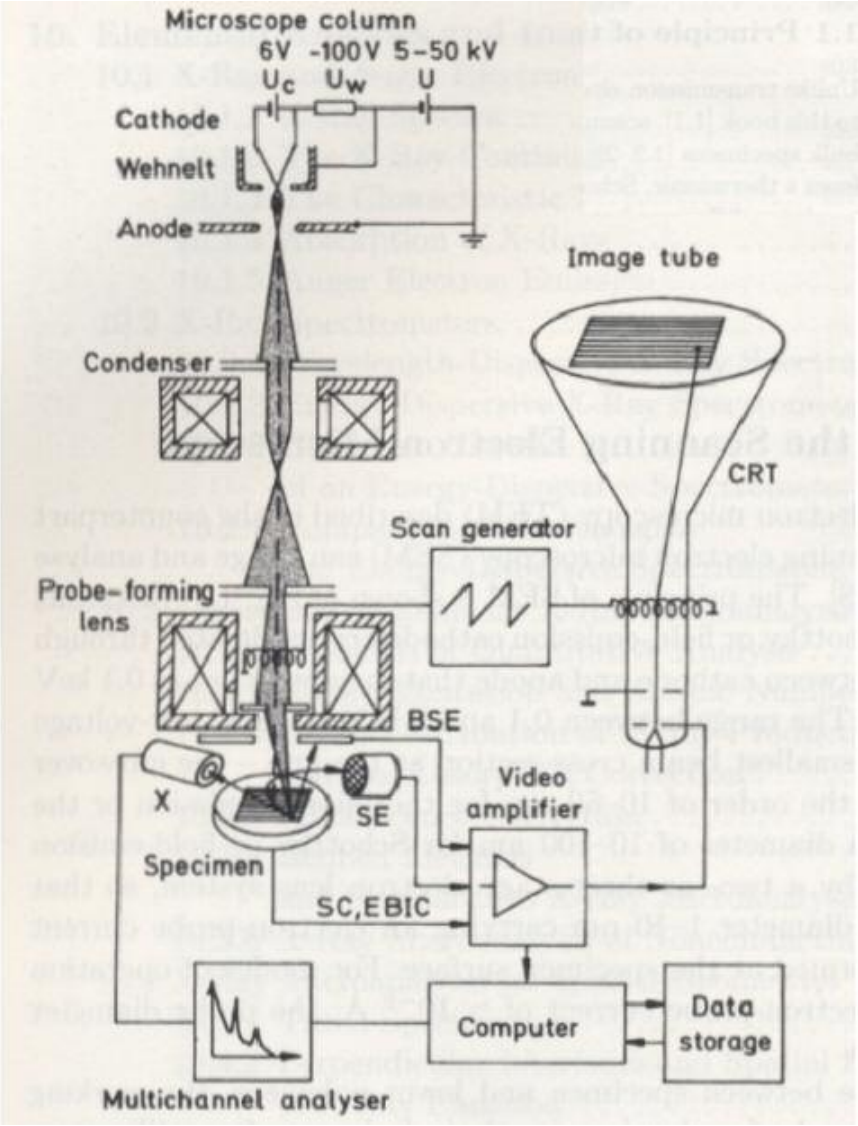

Figure 3.1 Principle of operation of the scanning electron microscope [13]

3.3 Electron Scattering

When the primary electrons hit the surface they interact with the sample's surface atoms to produce secondary electrons, backscattered electrons, x-rays, and Auger electrons. A secondary electron is an electron that is knocked out from the atom's core orbit or valence orbit when the incident electron hits the atom and transfers some of its energy to the electron, thereby giving one of the atom's electrons enough energy to escape from the orbit. When the secondary electron leaves the orbit a vacancy is created. If a higher level electron drops down into this vacancy, energy is released in the form of a single photon called an x-ray. Alternatively, this released energy can be transferred to another electron in the outer shell and this electron will have sufficient energy to leave the atom. These electrons are called Auger electrons, named for Pierre Auger, a French scientist who discovered the effect in 1921. A backscattered electron is an incident electron that is bounced back by colliding with another electron of one of the atoms on the surface. Backscattered electrons are deflected primary electrons, while secondary electrons come from the atoms on the surface of the sample

By analyzing the intensity of the scattered electrons a two-dimensional image of the surface can be constructed. Figure 3.2 shows different types of signals that are produced due to the electron beam and sample interaction, such as backscattered electrons, Auger electrons and x-rays; all of these can be used to analyze the sample's structure and composition.

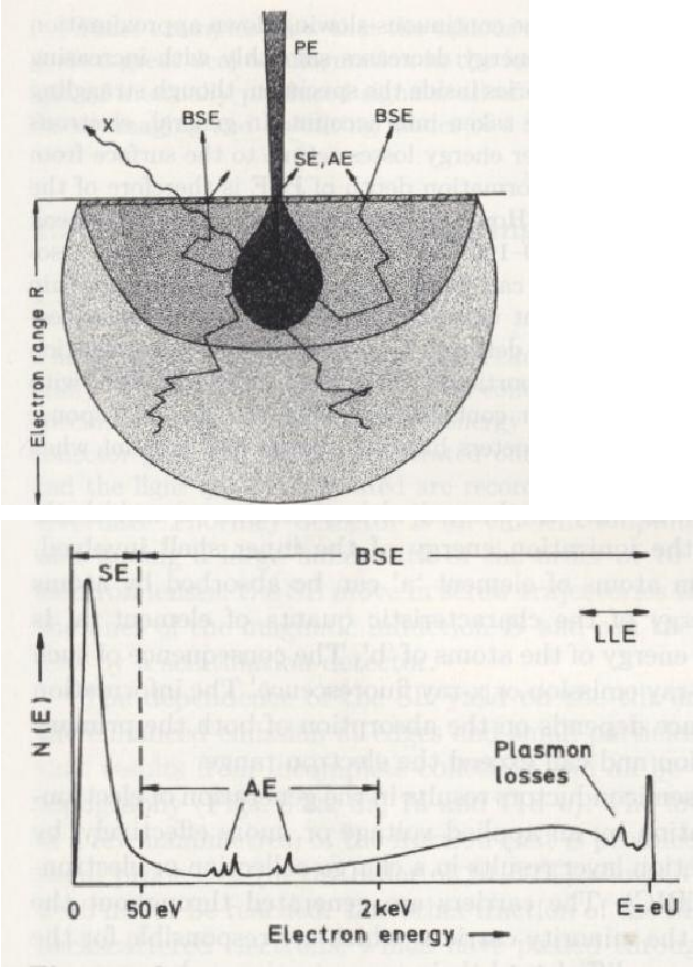

Figure 3.2 Electron specimen interaction diagram and energy spectrum of emitted electrons [13]

Chapter 4: NanoEDM: Experimental Setup

The experimental setup consists of three major parts integrated together (STM, SEM, and EDM). The full and the detailed views of the setup can be seen in figures 4.1 through 4.4. Figure 4.1 shows from left to right the SEM vacuum chamber, the SEM operational console, an oscilloscope, and a Nanoscope controller interface. The STM, the inchworm and the NanoEDM controllers, a frequency generator and a high voltage amplifier are positioned on top of the SEM console.

Figure 4.1 NanoEDM system complete setup

4.1 Description of Commercial Instruments

The scanning electron microscope (SEM) used in this experiment is a JSM-IC 848 manufactured by Jeol. The instrument used to control the scanning tunneling microscope (STM) is Nanoscope IIIa Scanning Probe Microscope controller manufactured by Digital Instruments. A slight modification was made to the Nanoscope controller. A BNC connection and a switch were installed on the front

panel, which allow an independent control of the Z-piezo voltage (before amplification). A voltage ranging from 0 to 11.8 volts can be supplied to the Nanoscope controller's high voltage amplifier by the NanoEDM controller during the EDM operation phase of the STM. The inchworm is controlled by a Burleigh 6000 ULN controller with a home-built remote control, which will be referred to as the inchworm controller. The frequency generator and a high voltage amplifier are used to generate a saw-tooth signal that controls an inertial motor. The function generator is manufactured by Hewlett Packard model 3312A. The bipolar operational power supply/amplifier is manufactured by Kepko model BOP 1000 M.

4.2 Description of Home-built Instruments

Figure 4.2 shows from left to right a larger view of the STM, the inchworm and the NanoEDM controllers. The circuit diagrams for these controllers are presented in Appendix B, and the pinout tables describing the connections between them are presented in Appendix A.

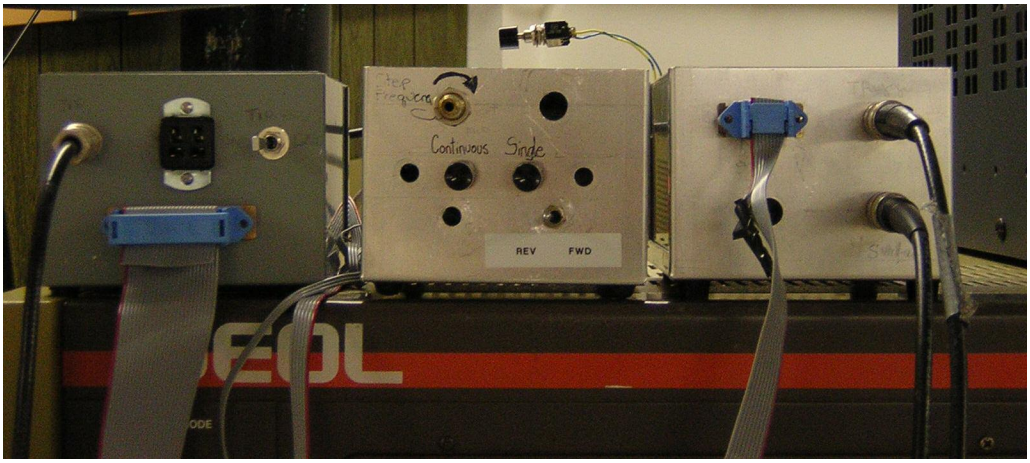

Figure 4.2 STM controller, Inchworm controller and NanoEDM controller

4.2.1 STM Controller

The STM controller is used to integrate all the signals and connect them to the STM/NanoEDM. The input to the STM controller comes from the Nanoscope controller. The STM controller separates the tip voltage line and sample bias line from the piezo scanner signals and sends them to the STM through separate BNC cables. This is done because the tip voltage and bias voltage are low compared to high voltages need to control the scanner. Therefore a crosstalk from the high voltage signals can result if these voltage lines are running in the same ribbon cable. The STM controller also modifies a motor activating signal and sends it to the inchworm controller. The Nanoscope controller was designed to use a dc motor for the coarse surface approach, but in our application we are using an inchworm motor for this function, therefore the signal has to be converted into a pulse sequence by a 555 timer in order for the approach mechanism to work properly. The STM controller also houses a switch that allows the tip to be grounded; this feature is needed for the EDM application. The power supply signals and the reference voltage for the NanoEDM controller also come from the STM controller.

4.2.2 Inchworm Controller

The Inchworm controller is used in conjunction with the 6000 ULN controller to operate the inchworm motor. Inchworm controller provides the capability for varying the speed of the motor and the direction of motion; it also allows the motor to run in two separate configurations: continuous step mode and single step mode. The inchworm controller takes the signal from the 6000 ULN and converts it into a pulse sequence with a 555 timer. The signal from the 6000 ULN is used to indicate the end

of the step, while the signal to start comes from one of the switches located on the inchworm controller.

4.2.3 Current Limiting Switch

Current limiting switch prevents arcing between the high voltage terminals of the inchworm motor in the 10^{-2} mbar vacuum region. Arcing occurs due to the polarized air molecules whose mean free path in low vacuum is long enough to create a chain of ionized molecules between a high voltage electrode and ground. The voltages used to control the inchworm motor are in the range of 200 to 400 volts and the spacing between the terminals is 5 mm. During ambient environment operation the air serves as an insulator between the high voltage terminals, because the mean free path of polarized air molecules is too short and the voltages are too low to create a dielectric breakdown. Once the vacuum is high enough, 10^{-4} mbar or better, the air molecules are spaced out far enough to prevent arcing. Therefore, during the vacuum pump-down of the SEM all high voltages need to be turned off. However, if we turn off the voltage to inchworm motor, the piezos that hold the load-bearing rod will relax and the tip will crash into the sample. To solve this problem, the current limiting switch limits the current flowing to the inchworm while keeping the voltages the same. Current is limited by channeling inchworm voltage lines through 22 MΩ resistors.

.

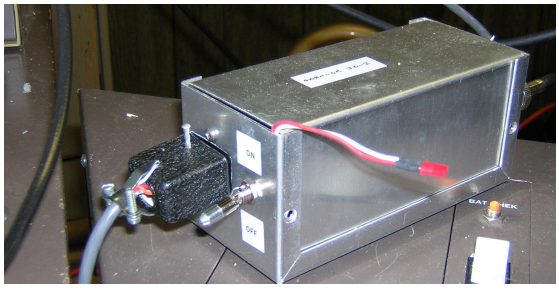

Figure 4.3 Current limiting switch for the inchworm motor

4.2.4 NanoEDM Controller

The NanoEDM controller controls the motion of the piezo scanner in the Z direction. It moves the tip towards the surface at a very slow speed and as soon as the current begins to flow it quickly withdraws the tip. During this process the tip is grounded and the bias voltage is set to a value ranging between 1 and 10 volts. The circuit compares the reference voltage to the actual voltage of the sample. When the tip is within several angstroms (Å) from the surface a current starts to flow between the tip and the sample and the bias voltage drops. This drop in the bias voltage serves as a trigger for the EDM controller to withdraw the tip. A similar result occurs when the tip actually touches the surface and a physical conduction channel is established. A capacitor is used to store energy that is transferred to the surface when the discharge takes place. The larger the value of the capacitor the more energy is released during the discharge. After the discharge takes place a small deformation appears on the surface. The Nanoscope controller is then switched back from the EDM mode to the STM mode in order to image the surface and analyze the deformation.

4.3 Description of STM

The actual STM positioned inside the SEM vacuum chamber is shown in figure 4.4. The parts numbered in this picture are listed below.

1. Tip current signal pre-amplifier circuit
2. Piezo tube scanner
3. Sample holder and gold sample
4. Tip current carrying vacuum-compatible coaxial cable

5. Voltage connections to the pre-amplifier
6. Voltage connections to the Inchworm
7. Voltage connections to the piezo tube scanner
8. Back limit inchworm switch
9. Piezo tube holder moved by inchworm (not visible)
10. Rollers
11. Stage position adjustment screws

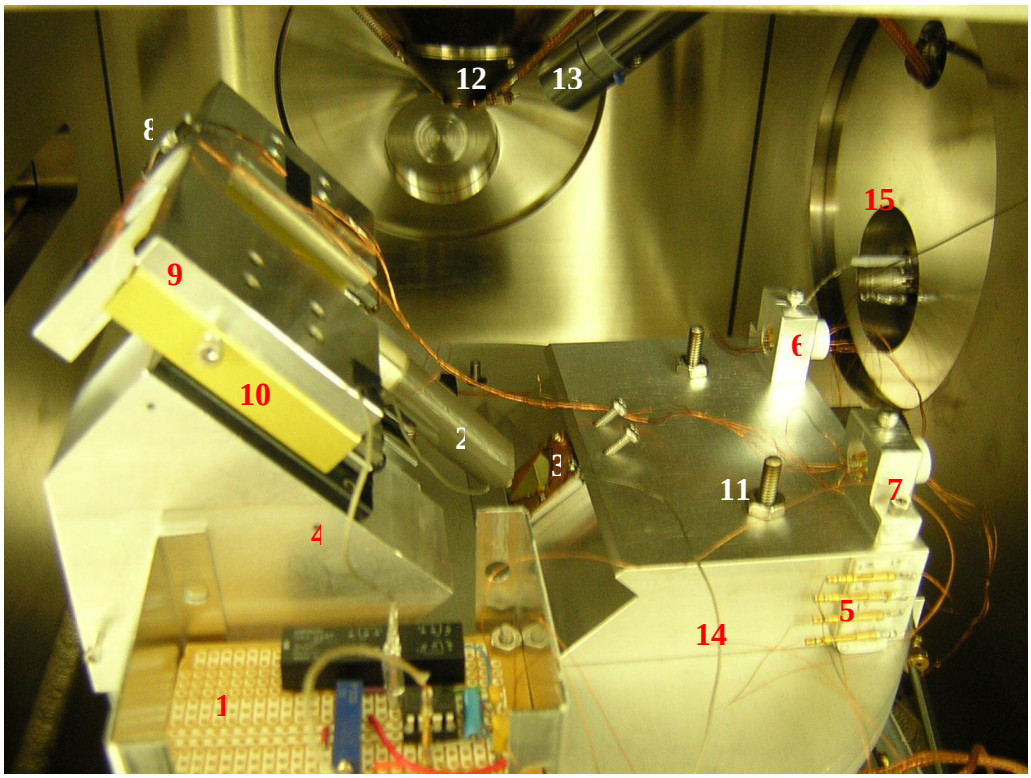

Figure 4.4 STM/NanoEDM system inside the SEM chamber

12. SEM electron beam column
13. SEM electron detector
14. Bias voltage carrying vacuum compatible coaxial cable
15. Flange with connectors

The AutoCAD drawings that were used to build the STM can be found in Appendix C. A schematic diagram of the STM and all the components is shown in figure 4.5.

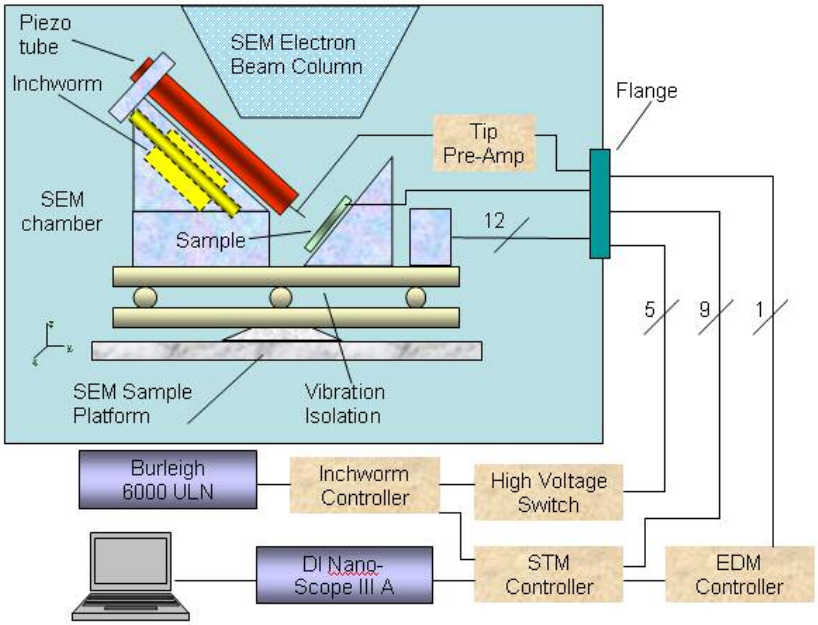

Figure 4. 5 Schematic diagram of the NanoEDM setup

4.4 Role of SEM in the Experiment

The SEM is used in this experiment as a vacuum chamber for the STM/NanoEDM system. Since the chamber does not have a camera attachment the SEM can be used to monitor the condition of the tip and observe changes that have been made to the surface after the discharge. After the inertial motor will be installed the SEM can also be used to monitor the position of the xy-stage. The SEM's chamber also proved to be extremely useful even during the operation of the STM in ambient environment. The SEM chamber's walls, made out of 1-inch thick steel provide a shield for the STM against the 60 Hz noise that comes from the other electronic equipment present in the room. Also the SEM chamber is supported by large springs that provide vibration isolation for the STM. Both of these issues, floor

vibrations and 60 Hz noise, were a significant problem in this experiment prior to placing the STM inside the SEM chamber.

4.5 Description of the Inertial Motor

In the present design the sample holder (xy-stage) is stationary and the maximum range for the NanoEDM is limited by the scanning range of the STM's scanner (about 100 µm wide). The NanoEDM range can be greatly extended with the implementation of an inertial motor. The inertial motor that can be used as an xy-stage is shown in figure 4.6.

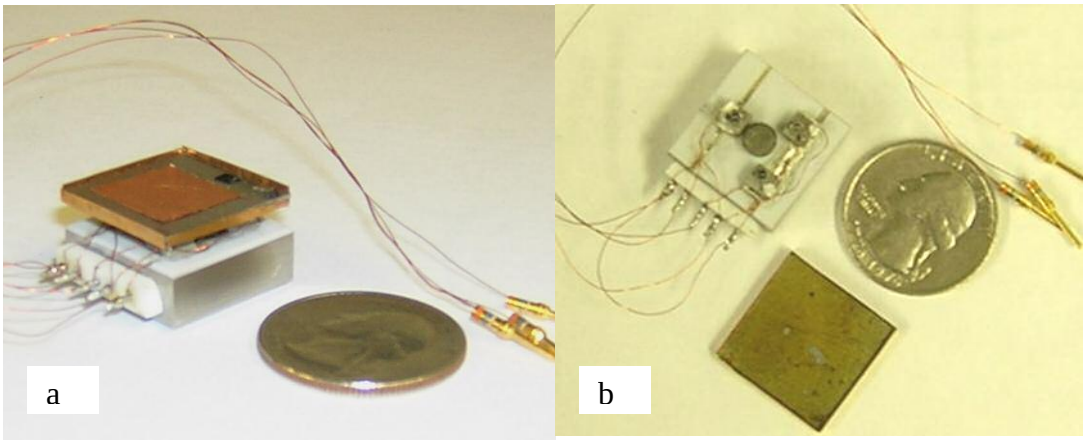

Figure 4.6 Inertial motor: a) full view and b) top view

The main principle of operation of an inertial motor is based on the difference between static and kinetic friction. An inertial motor operates by slowly shearing the piezo legs and then quickly contracting them back to the original form. When the legs are slowly sheared the stage that rests on top of them moves with them due to the static friction between the legs and the stage. When the piezos suddenly move in the opposite direction the inertial moment of the stage overcomes the kinetic friction and keeps the stage in place. As a result of this process the piezos remain in the original

location and the stage is displaced relative to them by less than a micrometre. The cycle is then repeated many times in order to achieve the desired displacement of the stage. The shearing and contracting of the piezos is controlled by a saw-toothed voltage signal applied to them. Each period of the signal corresponds to one step of the stage.

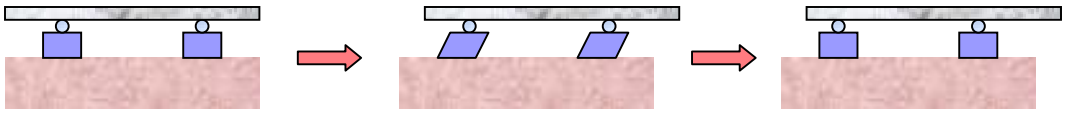

Figure 4.7 Schematic diagram of motion for the inertial motor

Three piezo stacks are used to translate the stage; they consist of two pieces of Ni coated piezo material oriented at 90° with respect to each other. The top layer moves the sage in x-direction and the bottom layer moves it in y-direction. The dimensions of the piezo pieces are 3x2 mm and the thickness is 1 mm. The middle part of the stack is ground and the top and bottom parts are connected to a high voltage source. The piezo pieces and copper wires are held together by a vacuum compatible conducting epoxy.

On top of each stack is a sapphire ball of 1 mm in diameter. The sapphire balls create a single point contact between the piezo stack and the stage. The bottom of the stage is covered with a thin glass slide to provide a smooth, scratch-free surface. The stage has small borders around it in order to prevent it from sliding off the stacks. Three stacks are used due to the geometrical principle that a unique plane can be drawn based on three points. If four stacks were to be used to support the stage, they would have to have identical height to ensure contact between each stack and the stage. In the geometrical center of the stacks triangle is a magnet adjustable by a

screw underneath. The magnet is used to keep the stage in place when the inertial motor is operated on an incline. The screw allows varying the height of the magnet and thereby the strength of the magnetic field needed to keep the stage from sliding.

A saw-tooth voltage pattern applied to the top or bottom of all three stacks simultaneously will translate the stage in either x or y direction, reversing the polarity of the voltage will translate the stage in the negative x or y directions. A frequency generator and a high voltage amplifier are used to produce the desirable voltage pattern. Increasing the amplitude or the frequency of the voltage will increase the translation speed. The voltage in the range of 50 V to 300 V has been found safe to operate the inertial motor at a frequency of 60 Hz. Decreasing the voltage will not result in shearing of piezos needed to move the stage, increasing the voltage may cause the dielectric breakdown of the piezo.

4.6 Procedure for Making a Discharge

Prior to making a discharge, the surface of the sample is scanned in a regular STM mode. This is done to insure that there are no large deformations present in the vicinity of the potential discharge spot. After a smooth area of about 5 µm wide is found the procedure for creating a discharge is as follows:

1. Set the scan range to zero.
2. While in STM mode withdraw the tip from the surface by setting the current set point to minimum value (2.99 pA). This causes Z piezo to contract and the tip to withdraw.
3. Withdraw the tip further away from the surface by making four steps back with the inchworm.

4. Switch the Nanoscope controller from STM mode to EDM mode. This disconnects the Z piezo voltage at the point before it enters the amplifier, and the EDM controller is used to control the Z piezo.
5. Disconnect the bias voltage line from the STM controller and connect it to the EDM controller.
6. Ground the tip.
7. Set the reference voltage to the desired value between 1 and 10 volts (usually 5V).
8. Insert the capacitor of the desired value into the EDM circuit.
9. Start the discharge approach. The EMD circuit slowly increases the voltage on the Z piezo until it is fully extended. If the current between the tip and the sample is detected during that time, meaning that the discharge has occurred, the tip withdraws quickly.
10. If the discharge did not occur, reset Z piezo voltage to minimum value, make one step forward with the inchworm, and repeat step 9.
11. After the discharge take 4 steps back using the inchworm.
12. Unground the tip.
13. Reconnect the bias voltage line back to the STM controller.
14. Set voltage, current and gain to the regular approach values.
15. Offset the center several microns away from the discharge point. This is done in order to avoid any changes happening to the place of discharge due to approach.
16. Switch Nanoscope controller from EDM mode to STM mode.

17. Approach the surface and stabilize the tip.
18. Move back to the x and y offset values where the discharge was created and image the surface.

This procedure is valid for both ambient and vacuum environment operations. For vacuum operation the SEM's chamber has to be pumped down for several hours prior to conducting the experiment so that a vacuum level of 10^{-4} mbar or better is established.

4.7 Procedure for Making Patterns Using Mechanical Contact

The procedure for making patterns using mechanical contact is as follows. The STM is used to approach the surface and image a large area on the surface of the sample to make sure that the sample is flat and does not have any deformation. Then, while still tunneling, set the scanning range to zero and move the tip to the desired position within the scanned area using the x and y piezo controls. Move the tip away from the surface using the inchworm motor by taking four steps back, until the tunneling current cannot be established. Approach the surface using the inchworm motor by taking several steps forward until the current begins flow again. The surface is then imaged and the produced modification is measured and recorded. The procedure is then repeated several times by offsetting the tip to different positions on the surface, until the desired pattern is produced. This procedure can be done in air or in vacuum.

4.8 Procedure for Etching Tungsten Tips

The geometry of the tip plays a crucial role in the EDM process. In order to

create uniform features on a sub-micron scale the tip needs to be extremely sharp and elongated and it has to be free of oxides on its surface. Commercially etched tungsten or platinum–iridium tips do not have the geometry appropriate for our experiment. Therefore home made tungsten tips were etched prior to each experiment, in order to avoid oxide accumulation on the tips. Figure 4.8 shows an SEM image of the etched tungsten tip manufactured by Veeco. Even though the tip is sharp enough to produce good STM images, its conical structure is too wide to create a sub-micron size feature during the discharge. The SEM image of the tip produced by our method can be seen in figure 4.9. It has a very long and narrow structure and is ideal for our purpose.

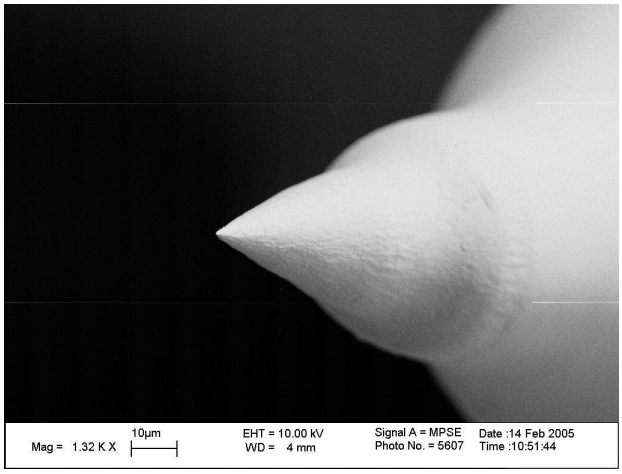

Figure 4.8 Tungsten tip manufacture by Veeco

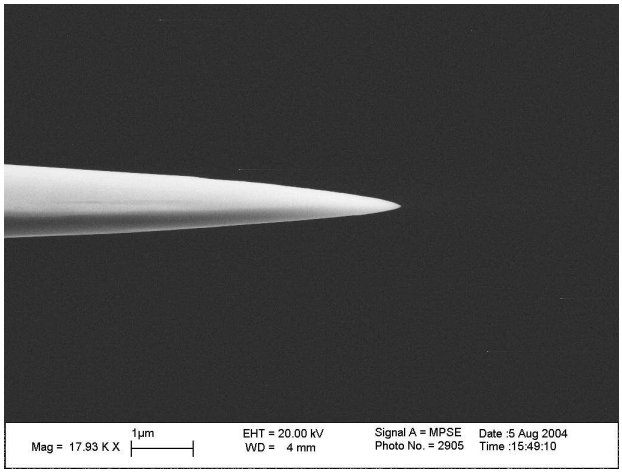

Figure 4.9 Home-made tungsten tip

The wire used to make the tips is W wire 0.25 mm in diameter and 99.98% pure. The etching solution was prepared by combining 100 mL of DI water and 7 flakes of potassium hydroxide (KOH). The tungsten wire was inserted inside the insulating tube, such as heat-shrink tube, and connected to an AC power supply. A copper coil was placed inside the potassium hydroxide solution and connected to the other end of the power supply. The insulation on the tungsten wire was separated into two parts with a small 5 mm long gap between them. Only the exposed part of the wire would be etched. The bottom part of the wire (containing the break in insulation) was placed in the center of the copper coil, so that the exposed gap was submerged in the solution. A small container was placed underneath the bottom part of the tungsten wire in order to catch the tip so that the tip would remain in the vertical position pointing upward after etching. The AC voltage used to etch the tip was on the order of 5 volts and the time duration of the etching process was between 5 and 10 minutes. After etching the tip was carefully extracted from the insulating tube and ultrasonically cleaned in acetone in order to remove the loose oxide flakes accumulated on the surface.

Chapter 5: Experimental Results and Discussion

5.1 STM Calibration

One of the stages of building the STM was calibrating the Nanoscope software. The STM had to be calibrated to make sure that the images I was seeing were of correct dimensions. In order to calibrate the software several samples with features of known dimensions were imaged, the dimensions of the features were measured and the scaling factors (measured in nm/volt) of the x, y, and z piezos were adjusted. The samples were then rescanned and the features were measured again to make sure that the adjustments were correct. To calibrate x and y piezo elements I used a diffraction grating that is commonly used in optical experiments. The spacing between gratings was measured to be 1µm. To calibrate z piezo we used a mica sample with a monolayer of microspheres deposited on it. The diameter of each microsphere is 1 µm. A thin layer of gold (200 nm) was deposited on top of both samples in order to make them conductive.

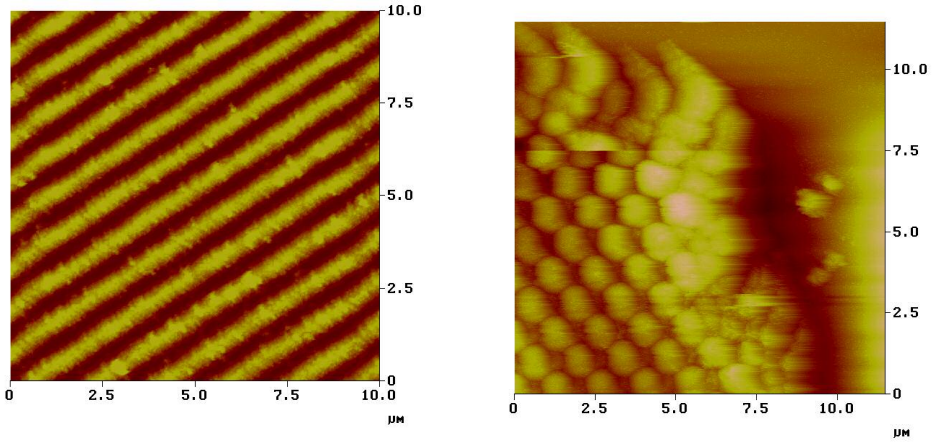

Figure 5.1 STM images of a diffraction grating (left) and microspheres on mica (right) used to calibrate STM (both samples are covered by a thin layer of gold)

5.2 Graphite sample

In the initial stages of building the STM a graphite sample was used for imaging. The advantage of using graphite is that it is very flat and the only things visible on the surface on a µm scale are steps. The graphite sample used in my experiment is a highly oriented pirolytic graphite (HOPG). HOPG is a material that consists of many atomic layers of carbon highly oriented among each other. This property makes HOPG an excellent tool for the STM calibration on a nm scale. HOPG is manufactured at a temperature of 3273K. It was tested that HOPG does not outgas at temperatures up to 600°C and remains stable at temperatures up to 2000°C in an inert environment. HOPG can be easily cleaved to expose a fresh conductive surface. The standard way to cleave graphite (and mica) is by using scotch tape to peel off the top layers. Figures 5.2 and 5.3 show graphite surface images of different dimensions that were obtained using my STM.

a) 

b) 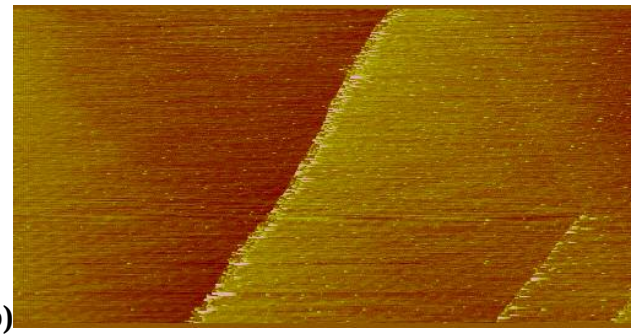

Figure 5.2 Graphite surface a) 40x20 µm b) 20x10 µm

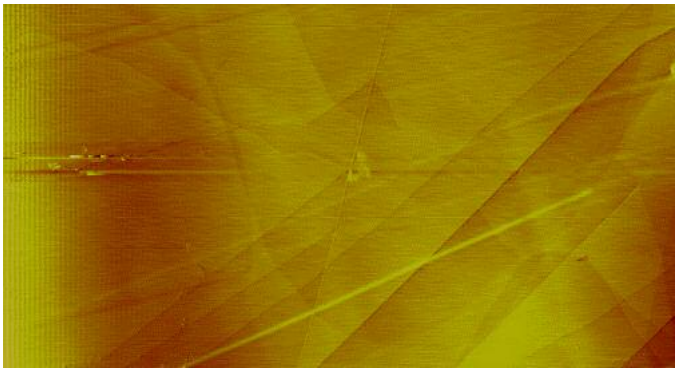

Figure 5.3 Graphite surface 10x5 µm

The best way to calibrate the STM on a nm scale is to use an HOPG sample. The atomic resolution of graphite reveals an hcp structure with well known dimensions. The center to center atomic distance is close to 0.1415 nm. Unfortunately, I was not able to obtain atomic resolution with my STM. As an exercise, the same sample was scanned using a DI STM with a short range scanner. Figure 5.4 shows an atomic resolution of graphite on a 5 nm and 10 nm scale. The scanner used in my STM is a long range scanner, and I suspect that vibration was the main cause for not being able to obtain atomic resolution.

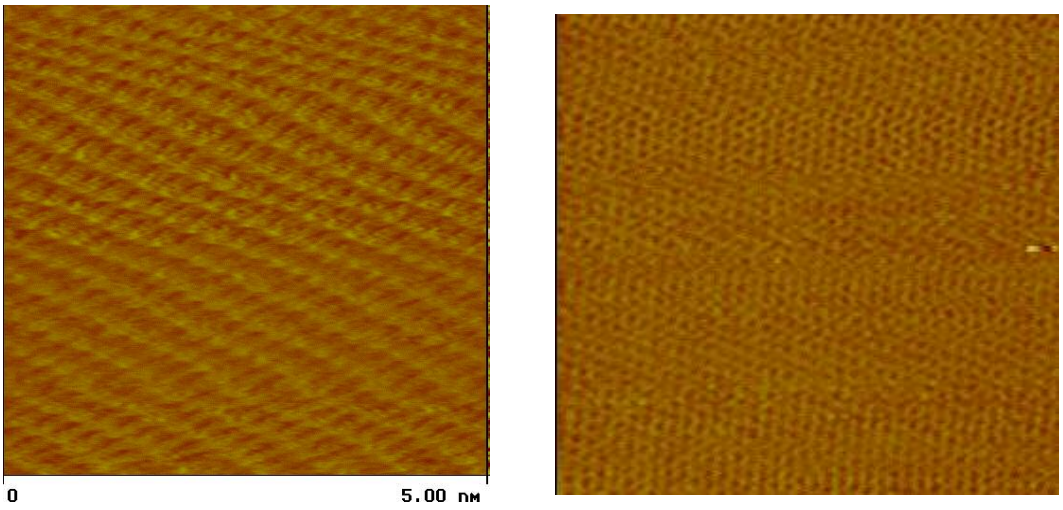

Figure 5.4 Atomic resolution of graphite (HOPG) obtained with a short range STM scanner in air: 5x5 nm (left) and 10x10 nm (right)

5.3 Gold Sample

The main goal of this experiment is to be able to produce deformations on gold surfaces. Therefore, when imaging the graphite surface became a routine procedure, the HOPG sample was substituted with a gold sample. The gold samples were produced by evaporating a thin layer of chromium on silicon substrate and then evaporating a thin layer of gold on top of that. The ratio of Cr to Au is 1:5, the thickness of the chromium layer was 10 nm and the thickness of the gold layer was 50 nm. The evaporation was done under vacuum, without exposure of the Cr layer to air before the gold layer deposition. Figure 5.5 shows images of the gold surface obtained in air and in vacuum using my STM.

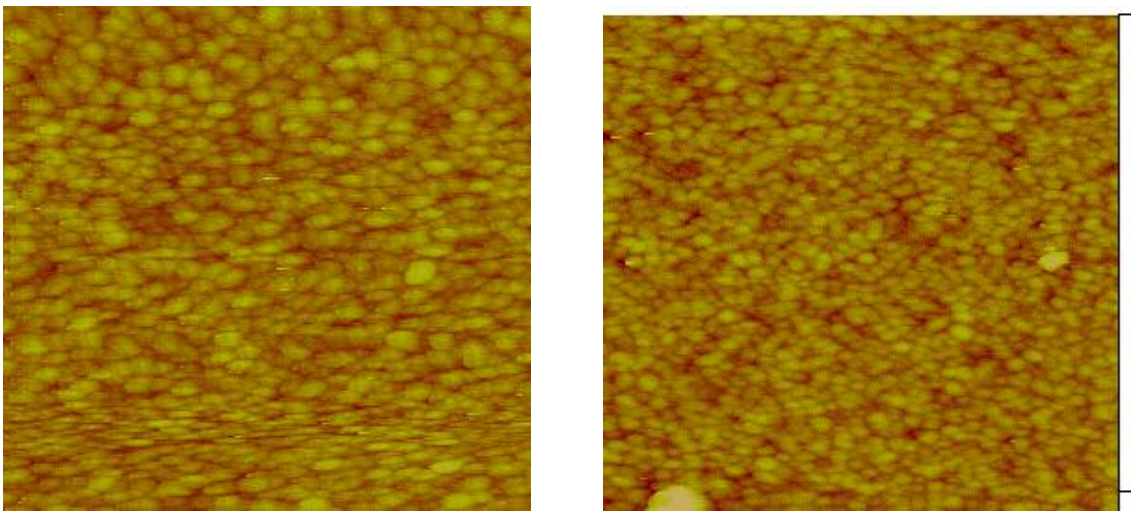

Figure 5.5 Gold surface images: 400x400 nm in air (left) and 1x1 µm in vacuum (right)

Both images clearly show gold crystallites that make up the gold surface. The average size of the crystallites is about 50 nm. When gold atoms are evaporated they land on the surface in many different spots at the same time. Each spot begins to grow in a different orientation that depends on the substrate on which it is growing, but is also somewhat random. As more gold is deposited on the surface the crystallites grow

larger. When a gold atom lands on the surface it has some energy to move around. However, this energy is not large enough to allow the atom to move to a different step on the surface. Therefore, when the atom lands on top of the crystallite it will remain there and effectively form a new layer. Also neighboring crystallites do not merge together if they have a different orientation. The result is a surface composed of many particles rather than of uniform layers. The size of crystallites depends on many different parameters, such as the vacuum level, temperature, rate of deposition, type of substrate and differences in evaporating procedures.

5.4 Surface Modifications: mechanical contact

I was able to modify gold surface in several different ways. One way do to it was by mechanical contact. Figure 5.6 shows a series of patterns with ridges across them created on a gold surface one at a time. The image below was obtained using an Atomic Force Microscope to confirm the results obtained with the STM.

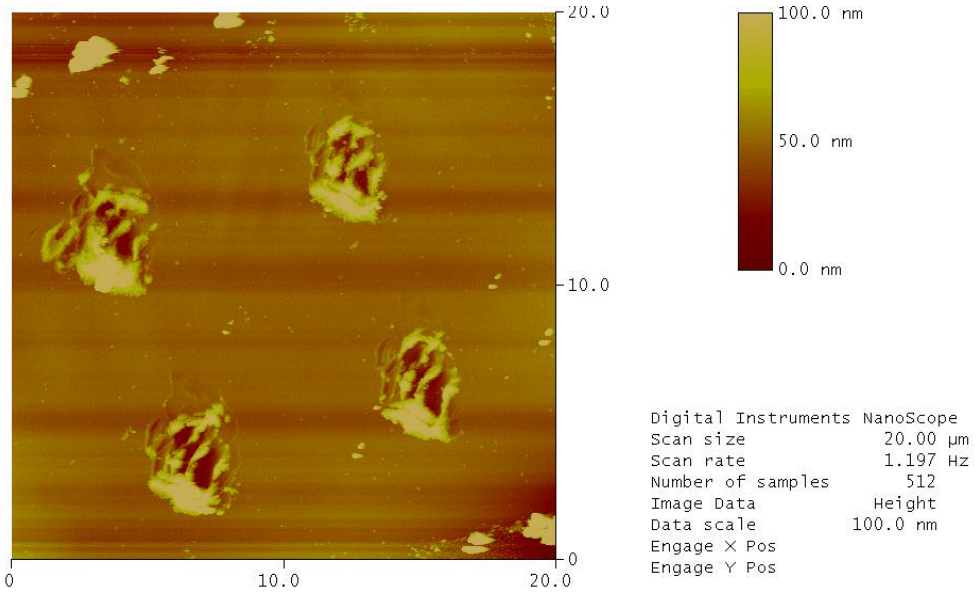

Figure 5.6 AFM image of a square pattern created by mechanical contact

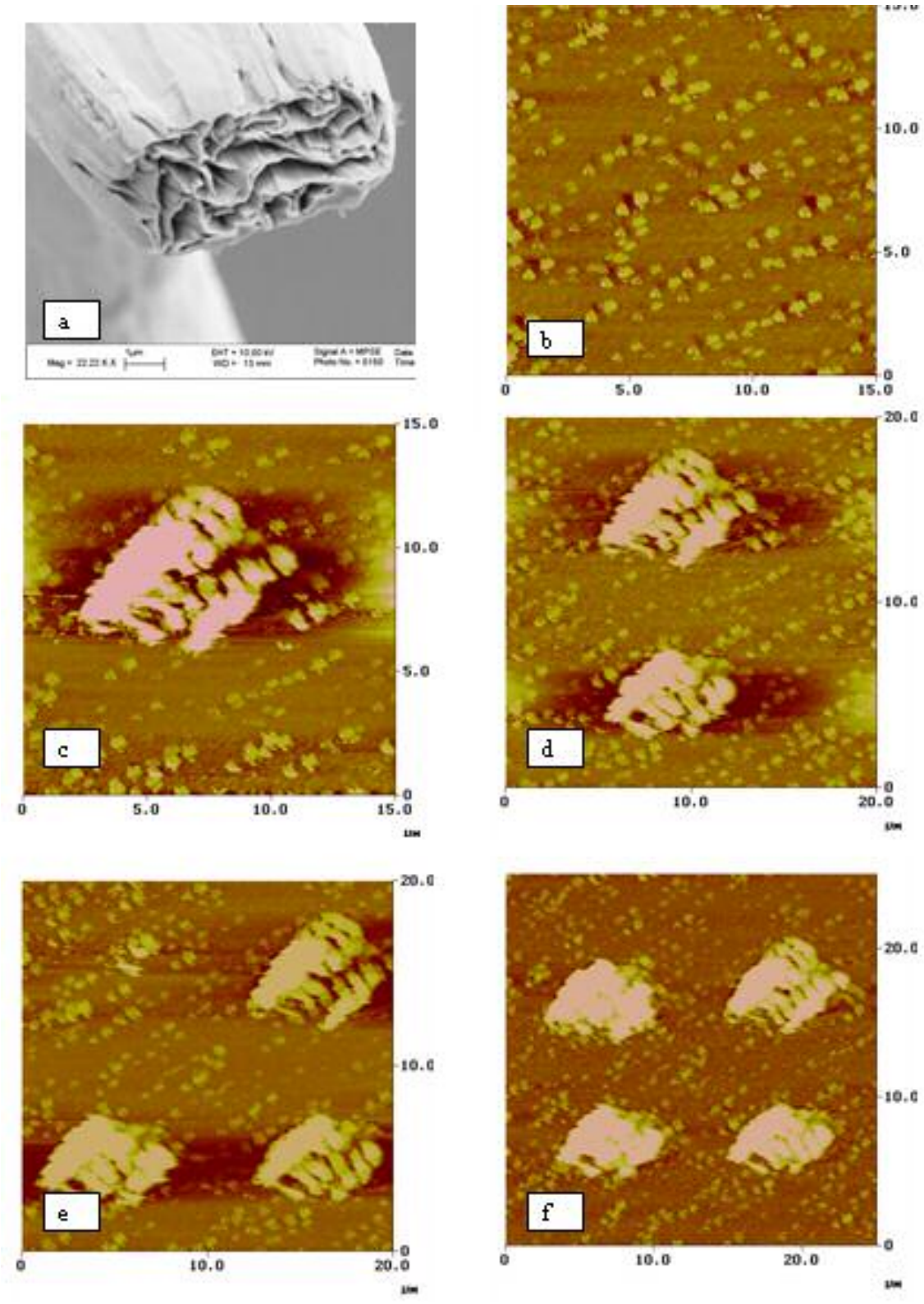

Figure 5.7 Patterns imprinted on gold surface with a clipped W tip and an SEM image of the tip

This kind of pattern was created with a clipped tungsten tip. The tip was made by a regular electro-etching method described in the previous chapter. The tip was then clipped under the microscope using cutting tweezers. Due to the layered structure of tungsten and its brittle properties clipping the end of the tip created a surface with ridges.

In the images in figure 5.7 found on the previous page the background surface appears to have many large particles on it, this is due in part to the dullness of the tip. Since the smallest feature any tip can resolve is the size of the diameter of the pinnacle of the tip itself, the small particles on the surface appear to be much larger than they really are.

The SEM image of the tip can be seen on the previous page in the first image (a) in figure 5.7. The second image (b) shows the gold surface before any modification took place, and the next four images (c-f) illustrate the appearance of imprints on the surface. The dimensions of the created features are consistent with the size and shape of the tip. The tip is rectangular with the dimensions of approximately 2x5 µm and the average size of the features produced by this tip is also ~2x5 µm. In this experiment the bias voltage was set to 500 mV and setpoint current was 30 pA, the experiment was conducted in ambient environment.

The relationship between the features and the STM tip geometry strongly suggests that surface modification due to mechanical contact results in an imprint of the tip itself. The variation between the individual features can be attributed to variation in pressure exerted by the tip during contact. Variations could have resulted from mechanical vibration of the tip or due to the differences in the angles that the tip

makes with the surface. This nevertheless shows the feasibility of stamping similar features using pre-designed tip geometry.

5.5 Surface Modification: discharge in air

Another way to modify the surface is to produce a discharge between the STM tip and the gold surface. The procedure for producing the discharge is described in detail in chapter 4. In contrast with mechanical deformation, features created using electrostatic discharge are significantly smaller. The radius of the craters ranges from 10 nm to 1 µm.

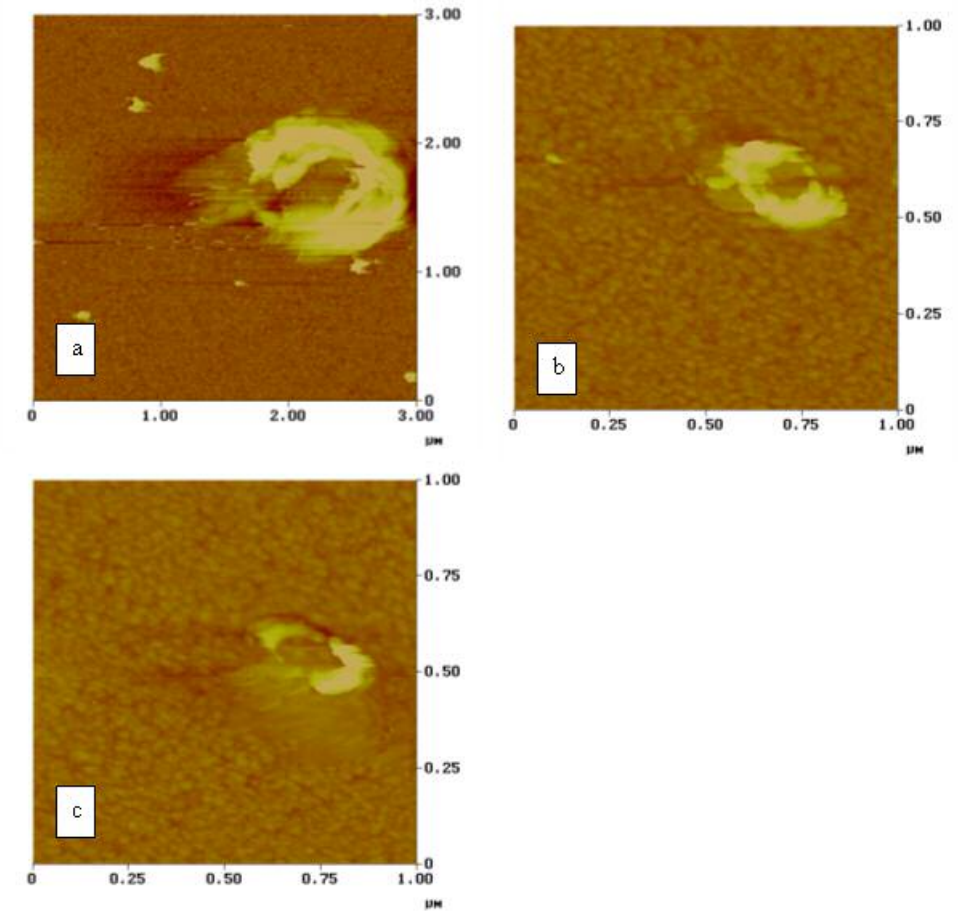

Figure 5.8 Craters created during discharges in air at 5 volts a) 200 nF double discharge b) 200 nF single discharge and c) 100 nF single discharge

Figure 5.8 shows several craters of different dimensions produced during such discharges. The voltage was set to 5 volts and the capacitance varied in the nF range. Very sharp tungsten tip made on the day of the experiment was used to ensure minimal oxidation of the tip.

By correlating the size of the crater with the value of the capacitor used in the circuit, it can be shown that the dimensions are increasing with the capacitance. Table 5.1 shows the data obtained from several experiments. Since the craters appear to be elliptical in shape the dimensions are given in terms of major (2a) and minor (2b) axes and the total area of deformation is calculated by equation 5.1.

$$A_{ellips} = \pi ab = \frac{\pi}{4} WL \qquad (5.1)$$

Table 5.2 Correlation between capacitance values and dimensions of craters produced in air

Capacitance	Dimensions	Total area	# of discharges
10 nF	70 x 40 nm	2198 nm^2	1
100 nF	330 x 130 nm	33677 nm^2	1
215 nF	280 x 200 nm	43960 nm^2	1
215 nF	1.2 x 1 µm	942000 nm^2	2
450 nF	0.9 x 0.6 µm	423900 nm^2	1
1 µF	2 x 0.7 µm	1099000 nm^2	1
4.7 µF	4.5 x 1.5 µm	5416500 nm^2	1

The plot of the data from table 5.1 for all the single discharges can be seen in figure 5.9 on the next page. A straight line is fitted to the data. The dependence of the modified surface area on the capacitance appears to be linear in the specified range.

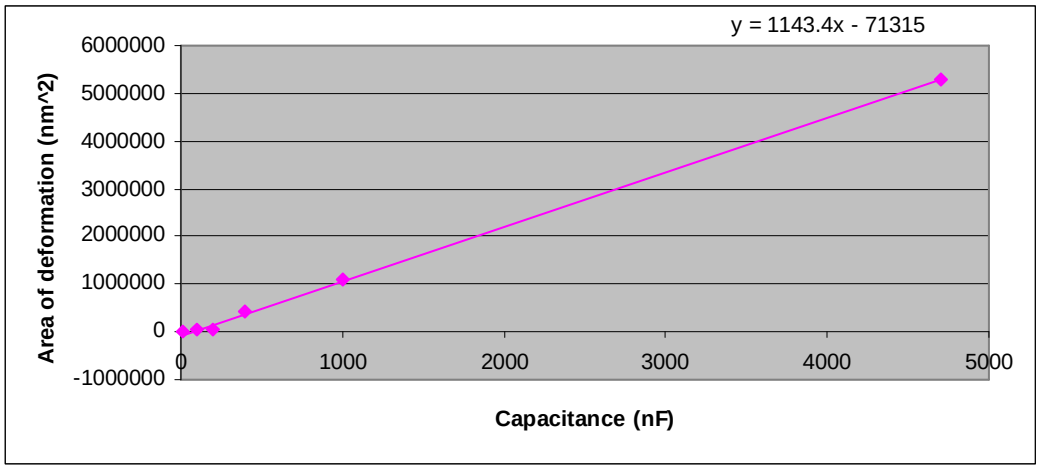

Figure 5.9 Capacitance value vs. area of deformation of gold surface during discharge in air

The maximum value of the capacitance is limited in this experiment to 4.7 µF due to circuit constrains (larger capacitors take more time to saturate, therefore disrupting the timing of other processes). At larger values of the capacitors the tip would reach the surface without triggering a discharge. The other limiting value of 10 nF was imposed by the resolution of the STM itself and the quality of the gold surface. The craters produced at 10 nF or less were comparable in size to deformations randomly found on the surface and therefore craters of smaller size would be indistinguishable from random deformations.

5.6 Surface Modification: discharge in vacuum

The third way to modify the surface is by making discharges in vacuum. The square patterns were created by a similar procedure as described before in section 4.6. The only difference was that after step 11 was completed the system remained in the EDM mode while the tip was repositioned over a new place, usually 1or 2 µm away from the original position and a second discharge was created. This step was repeated four times in a row before converting the system back to the STM mode. The results

of these experiments can be seen in figure 5.10. As in the previous section the voltage was set to 5 volts and the capacitance was varied between 10 and 400 nF.

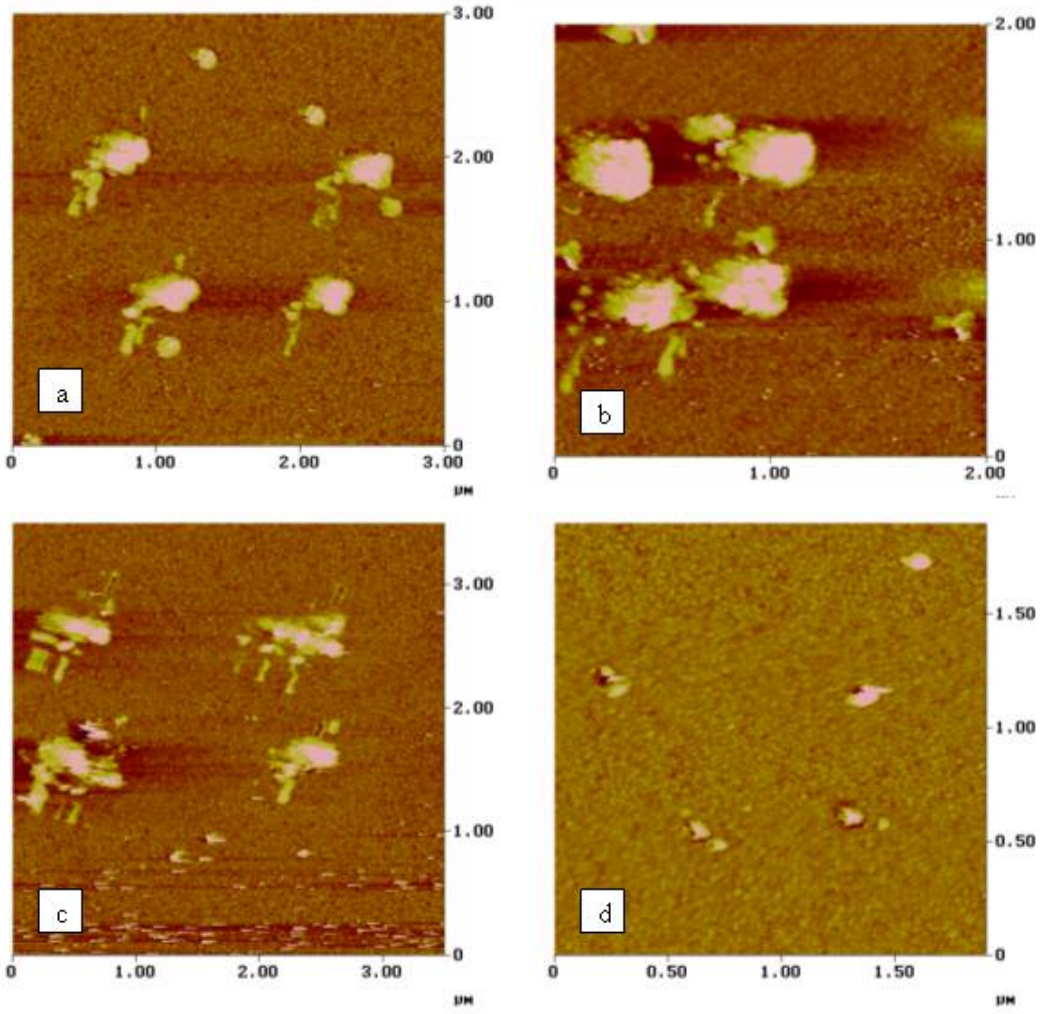

Figure 5.10 Square patterns produced by discharges in vacuum at 5 volts a)100 nF 1.5 µm apart b) 100 nF 1 µm apart c) 200 nF 2µm apart d)10 nF 1µm apart

From these images it can be seen that the mechanism for creating a deformation is different between ambient and vacuum environment. In ambient environment only craters are created during discharges. However, in vacuum during the discharge some material is also being deposited on the surface, forming a mound. Table 5.2 shows the capacitance values correlated with the volume of the mounds produced by discharges in vacuum.

Table 5.2 Correlation between capacitance values and volume of mounds produced in vacuum

Capacitance (nF)	Width 2a (nm)	Length 2b (nm)	Height c (nm)	Volume (nm^3)
10	134	155	85	925095.8
10	118	80	44	217648.64
10	68	105	50	187068
10	89	133	40	248103.52
50	500	177	61	2828814
50	325	130	54	1195506
50	230	100	34	409768
50	400	140	41	1203104
100	320	330	92	5090764.8
100	360	300	76	4300992
100	290	260	52	2054499.2
100	370	300	68	3955152
100	445	270	95	5981067
100	460	247	96	5715540.48
100	380	300	92	5495712
100	460	288	87	6039498.24
200	621	266	60	5193447.84
200	840	360	63	9982828.8
200	506	305	61	4933004.12
200	810	240	53	5398876.8
450	1300	700	100	47684000
450	1000	440	91	20980960
450	900	346	60	9790416
450	860	280	92	11608486.4

The volume of a mound is calculated based on the approximation that the mound has a shape of an ellipsoid sliced in half. The formula for calculating the volume of an ellipsoid is given in equation 5.2

$$V_{ellipsoid} = \frac{4\pi abc}{3} \tag{5.2}$$

Rewriting this formula for our purposes gives us equation 5.3

$$V_{\frac{1}{2}ellipsoid} = \frac{\pi}{6} WLH \qquad (5.3)$$

Figure 5.11 shows a plot of capacitance values vs. the volume of mounds. A straight line can be fitted to the data.

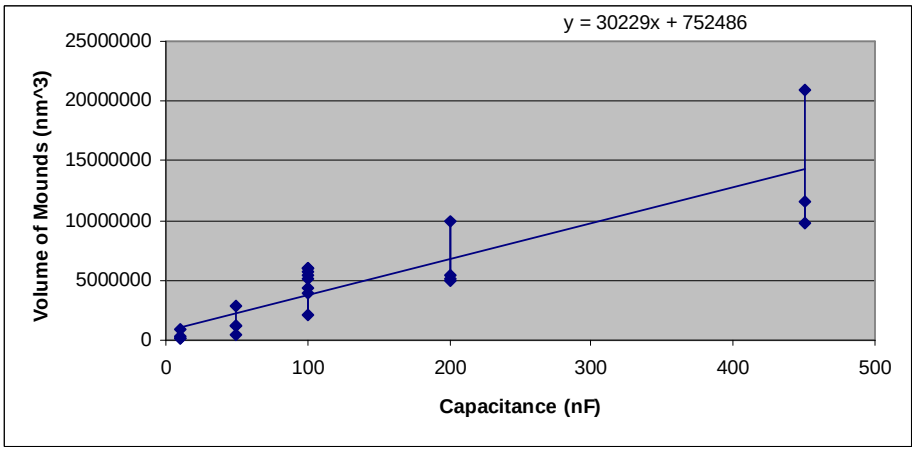

Figure 5.11 Capacitance values vs. volume of mounds deposited on gold surface during discharge in vacuum

This result agrees with the equation 5.4, which shows that the energy of the discharge is directly proportional to the capacitance.

$$E = \frac{1}{2} CU^2 \qquad (5.4)$$

Figure 5.11 shows that the volume of mounds is directly proportional to the capacitance and therefore is directly proportional to the energy of the discharge. This result is consistent with the theory that the energy requited to remove a given amount of material is equal to the energy required to remove one atom multiplied by the number of atoms (E_N=N*E_1). Therefore, the energy of the discharge is transformed into the energy required to produce a mound, by either removing material from the tip or from the surface.

5.7 Nature of Mounds

Ideally, we wish to create patterns that are exclusively craters of identical size without the presence of mounds. The experiments however show that the mounds are necessary byproducts of the process. Thus, it is of importance to understand what they are and if possible eliminate them.

The mounds can be composed of gold removed from the surface, tungsten or tungsten oxide removed from the tip. The composition can be determined by examining the modified surface with an energy dispersive x-ray analysis (EDX). However, it may also be possible to understand their nature through a series of experiments. For example, annealing the tip above 1500 ºC would eliminate oxide from the tip and thus, the mounds if they were oxides, would not be produced during the discharge. Similarly, the mounds may be bound weakly enough that post processing steps such as a mild plasma etching can be used to remove them.

The adhesion between mounds and surface was investigated in the following experiment. Figure 5.12 shows two images of the same pattern taken 15 hours apart from each other while the area was being continuously scanned at 0.4 Hz. It can be seen that over time the mounds became smaller or disappeared completely. The mounds seen in this figure were produced at 5 volts and 450 nF and the spacing between them was 1 µm. Since the area was being scanned continuously during the 15 hour time period it is not unreasonable to assume that the mounds were simply wiped away by the tip itself. What is interesting here is the fact that the removed material was transferred back to the tip. This assumption can be confirmed by looking at figure 5.13, which shows a series of mounds that were produced right after the

previous image (5.12 b) was taken.

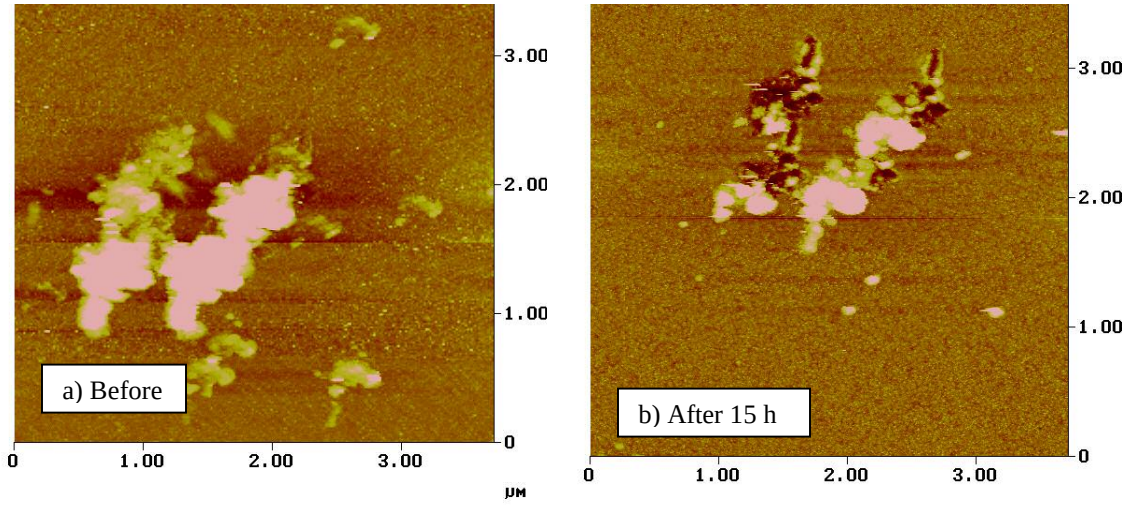

Figure 5.12 Images of the same area taken 15 hours apart show a significant reduction in the size of mounds

It can be seen clearly that the first two mounds in figure 5.13 are much larger than the next two. In fact, the volume of the first mound is five times larger than the volume of the last mound. This suggests that the material removed from mounds earlier was loosely attached to the tip and was deposited back to the surface during the discharge. In this figure the mounds were produced at 5 volts and 450 nF with a spacing of 2 µm between them.

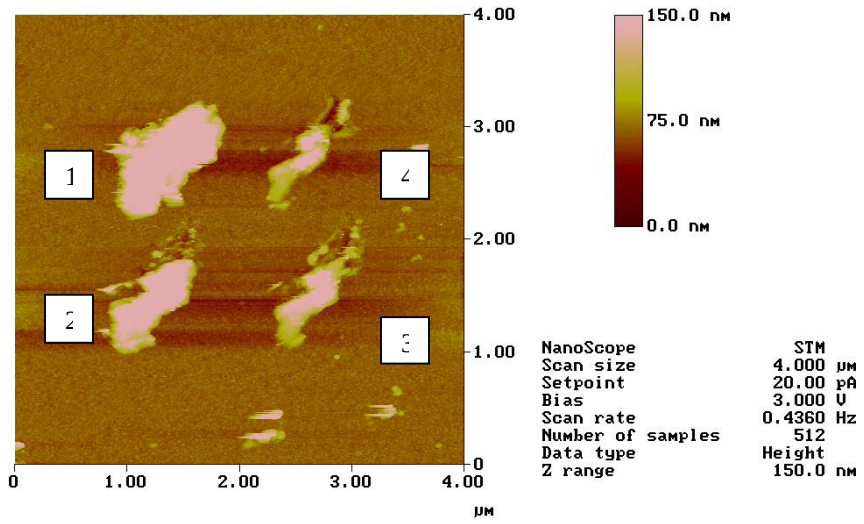

Figure 5.13 Reduction in the size of mounds after each consecutive discharge

Another insight into the nature of mounds comes from looking at the AFM images of the areas scanned previously by STM. As can be seen in figure 5.14 the surface inside the rectangular area with craters looks very clean compared to the surface outside the rectangle. Also, the area scanned by the STM is surrounded on the left and right sides with borders composed of the particles that were removed from the center.

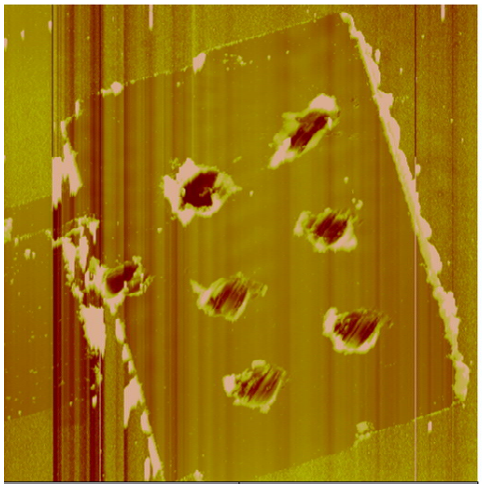

Figure 5.14 STM tip pushes particles on the surface to both sides of the scan area

The gold sample used in this experiment was exposed to air and did not undergo any sophisticated treatment to clean the surface before the experiment. It is safe to conclude that the particles accumulating on the sides of the scan area come from the contaminations present on the surface. These particles are picked up by the tip and can settle on both sides of the image or accumulate on the tip. The particles that accumulate on the tip can be deposited back on the surface during the discharge. If a discharge is produced without scanning the area before-hand, the result is usually a very clean crater like the ones seen in figure 5.15.

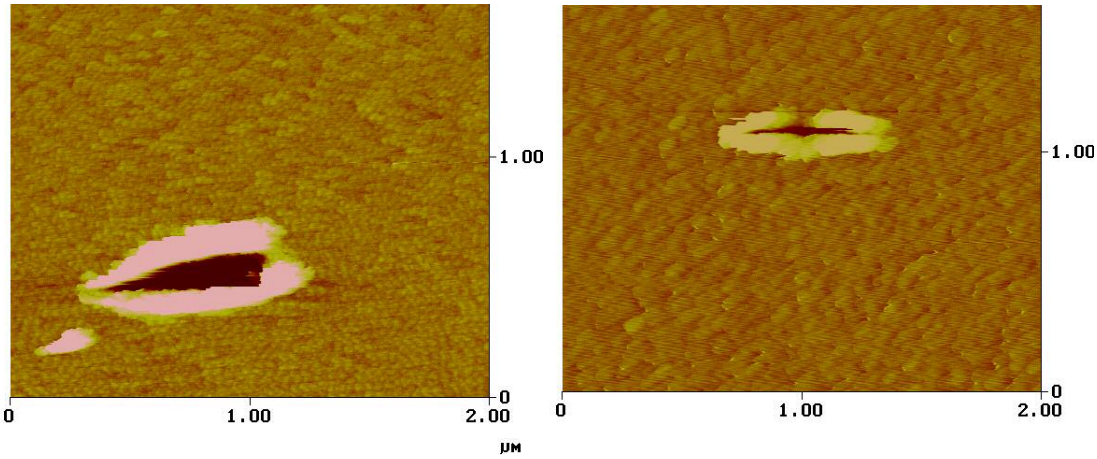

Figure 5.15 Discharges produced without the initial scanning of the surface do not create mounds

It can be seen from figure 5.12b that when the mounds are removed from the surface the craters underneath are exposed. Formation of craters underneath the mounds suggests that there is a crucial difference between discharges in air and in vacuum. In air, a mound forms around the rim of the crater, while in vacuum, the mound is formed above the crater. The rim formation in air is explained by the superheating theory discussed in section 1.4. The plasma channel in air is under high pressure is due to the thin layer of water present on the surface of the sample that acts as a dielectric fluid. The water layer is vaporized locally during the discharge creating a high pressure bubble. The pressure inside the plasma channel forces the molten material away from the center of the discharge, creating crater walls. However, in vacuum, the plasma channel is expected to have a much smaller pressure due to the absence of the water layer and lack of gas molecules. The pressure of the plasma channel in vacuum is insufficient to drive the molted material away from the center of the discharge. Therefore, the molten material will remain in the center of the plasma channel and will form a mound above the crater.

Conclusion

In the course of this experiment a new system called NanoEDM was designed and built. This new system is composed of three separate instruments STM, SEM and EDM. Original designs were used to build STM and EDM and the SEM had to be modified to accommodate the installation of the new system. The STM was designed specifically to be able to fit inside the SEM and to be oriented in such way that both the sample and the tip would be located directly underneath the electron beam column. This design allows both the tip and the sample to be imaged by the SEM. The EDM system was designed to be integrated with the STM system and to use Nanoscope controller's signals for its operation. The home-built STM instrument is capable of imaging different substrates, specifically gold and graphite (HOPG). It is capable of obtaining accurate images that range in width from 500 nm to 80 μm. It can also accurately resolve large deformations on the surface, as high as 100 nm.

The NanoEDM system is capable of producing deformations on the gold surface by several different methods. Imprints of the tip were created on a gold surface by mechanical contact between the tip and the surface. Craters were produced during discharges in ambient environment. Craters and mounds were produced during discharges in vacuum. The capacitance value in the EDM circuit can be varied from 10 nF to 4.7 μF and voltage values can range from 1 to 10 volts. The smallest deformation that I was able to produce in air was 60 nm in diameter. And the smallest deformation that I produced in vacuum was 100 nm in diameter.

Future work

It would be of interest to continue this experiment and to observe the effect other parameters might have on the dimension and shape of the deformations. One of the parameters that can be monitored is voltage, which can be varied from 1 to 10 volts. The polarity and range of the voltage can also be changed with additional modifications to the setup. Also, the oxidation of the W tips can be reduced by annealing the tips at 1500 °C. However, the tip will still be exposed to ambient environment during the transfer from the evaporation chamber (were it was baked) to the STM. More rigorous methods can be used to achieve a clean gold surface, such as annealing. Annealing of gold surface can be done in a separate set up and the sample then transferred to the STM. Also, with some additional modification to my system a heater can be installed underneath the STM sample holder that can be used to anneal the sample. This modification can produce really good results since the gold surface will be flattened and the water layer will be removed if the annealing is done in vacuum.

One of the modifications that can significantly impact the experiment would be to incorporate the inertial motor into the STM set up. With the inertial motor serving as a sample holder, the scanning range of the system can be increased from 100 µm to more than a centimetre. Increased range would allow for creation of more complex patterns on the surface as well as longer periods of continuous operation in vacuum without the need to manually reposition the tip over a new area.

Overall, the present experimental set up offers a wide range of possibilities that can be implemented to conduct future experiments.

Appendix A: Pin Connections Tables

Table 1: STM controller to Nanoscope IIIa connections

Pin #	Description	Pin #	Description
1	No connection	20	+5 V
2	No connection	21	No connection
3	No connection	22	Inchworm Controller
4	No connection	23	No connection
5	- Y electrode	24	+ Y electrode
6	No connection	25	No connection
7	- X electrode	26	+ X electrode
8	No connection	27	No connection
9	- 15 V	28	+ Z electrode
10	No connection	29	No connection
11	Tip voltage (amplified)	30	+ 15 V
12	Ground	31	Sample bias

Table 2: STM controller to SEM flange connections

Pin #	Description	Pin #	Description
3	No connection	16	+ 5 V
4	+ Z electrode	17	+ X electrode
5	+ Y electrode	18	- X electrode
6	- Y electrode	19	Ground
7	+ 15 V	20	- 15 V
BNC 1	Tip voltage (amplified)	BNC 2	Sample bias

Table 3: STM controller to NanoEDM controller connections

Pin #	Description
1	Sample bias
2	- 15 V
3	+ 5 V
6	Ground
7	+ 15 V

Table 4: 6000 ULN to Inchworm Controller connections

Pin #	Description	Pin # (6000 ULN)
1	Ground	2
2	+ 5 V	1
3	Enable	18
4	FWD/REV	19
5	Halt/Run	6
6	Clock	7
7	+ 5 V	14
8	Trigger 1	5
14	Trigger 2	8
15	Ground	15

Table 5: SEM flange connections

Pin #	Description	Pin #	Description
1	Center element	8	+ X electrode
2	Clamp element 2	9	+ Y electrode
3	Clearance compensation	10	- X electrode
4	Clamp element 1	11	- Y electrode
5	Reverse limit switch	12	Ground
6	+ 5 V	13	+ 15 V
7	+ Z electrode	14	- 15 V
BNC 1	Tip voltage (amplified)	BNC 2	Sample bias

Table 6: Inputs to STM (1 and 2)

STM Plug 1 (left)		STM Plug 2 (right)	
Pin #	Description	Pin #	Description
1	+ X electrode	1	Center element
2	- X electrode	2	Clamp element 2
3	+ Y electrode	3	Clearance compensation
4	- Y electrode	4	Clamp element 1
5	+ Z electrode	5	Reverse limit switch
6	Ground	6	+ 15 V
7	+ 5 V	7	- 15 V

Appendix B: Circuits Schematics

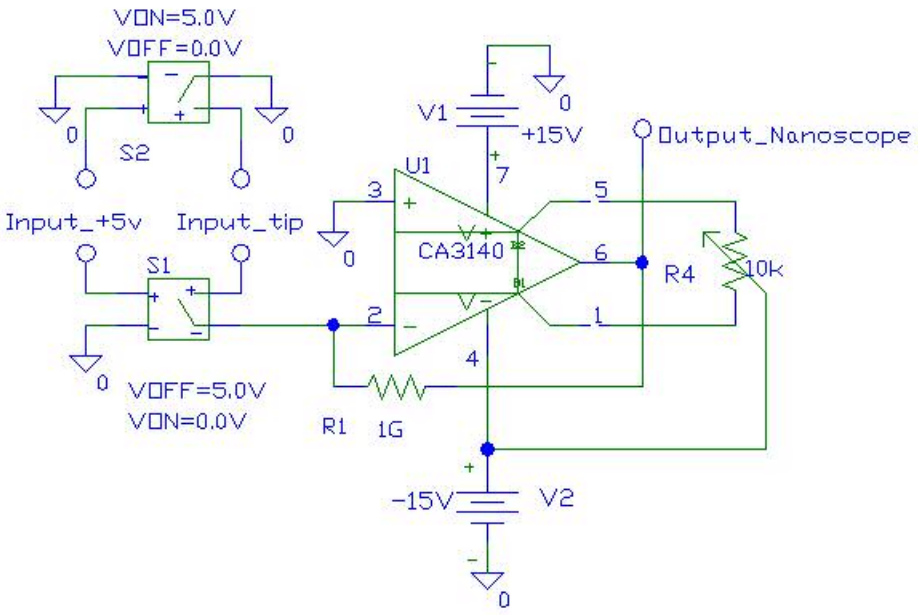

Circuit Schematic 4. STM tip voltage preamplifier circuit layout

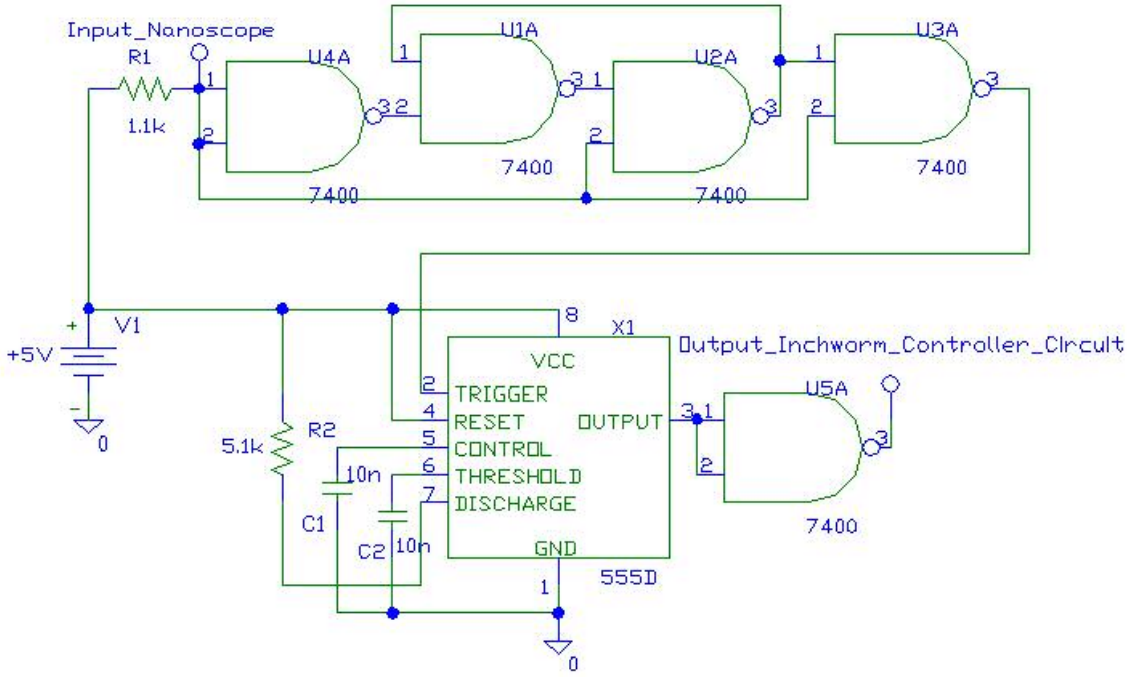

Circuit Schematic 5. STM controller circuit layout

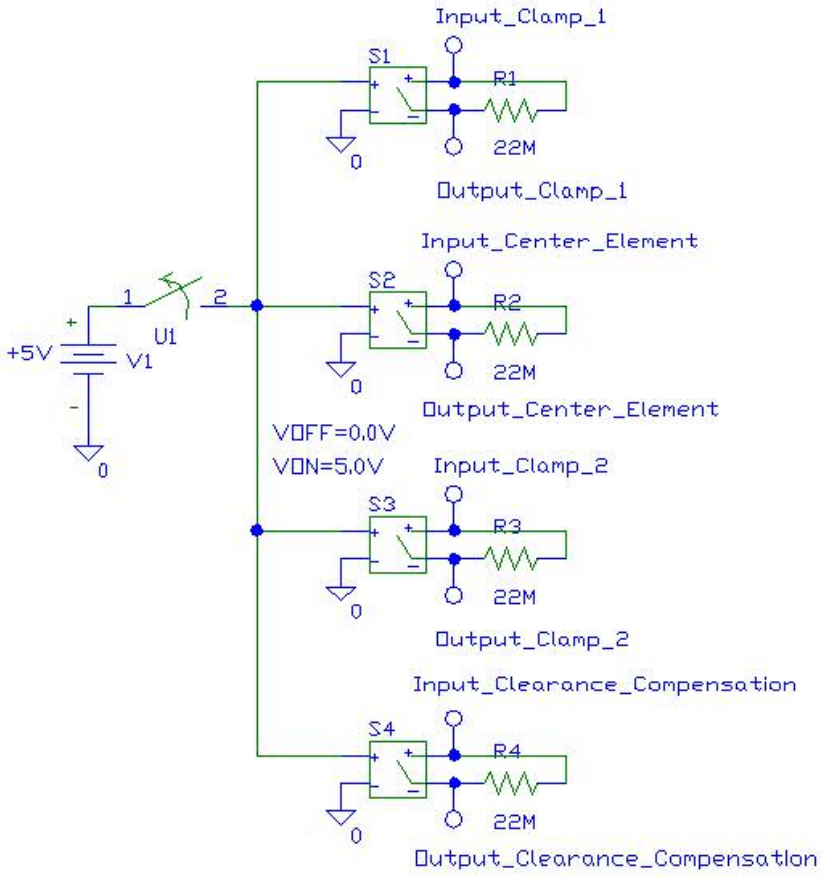

Circuit Schematic 6. Inchworm high voltage switch circuit layout

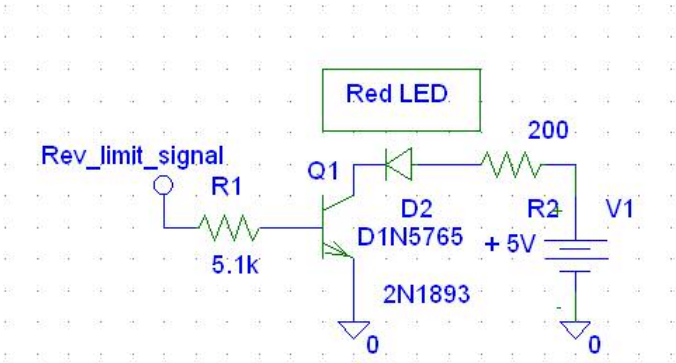

Circuit Schematic 7. Reverse limit indicator circuit layout

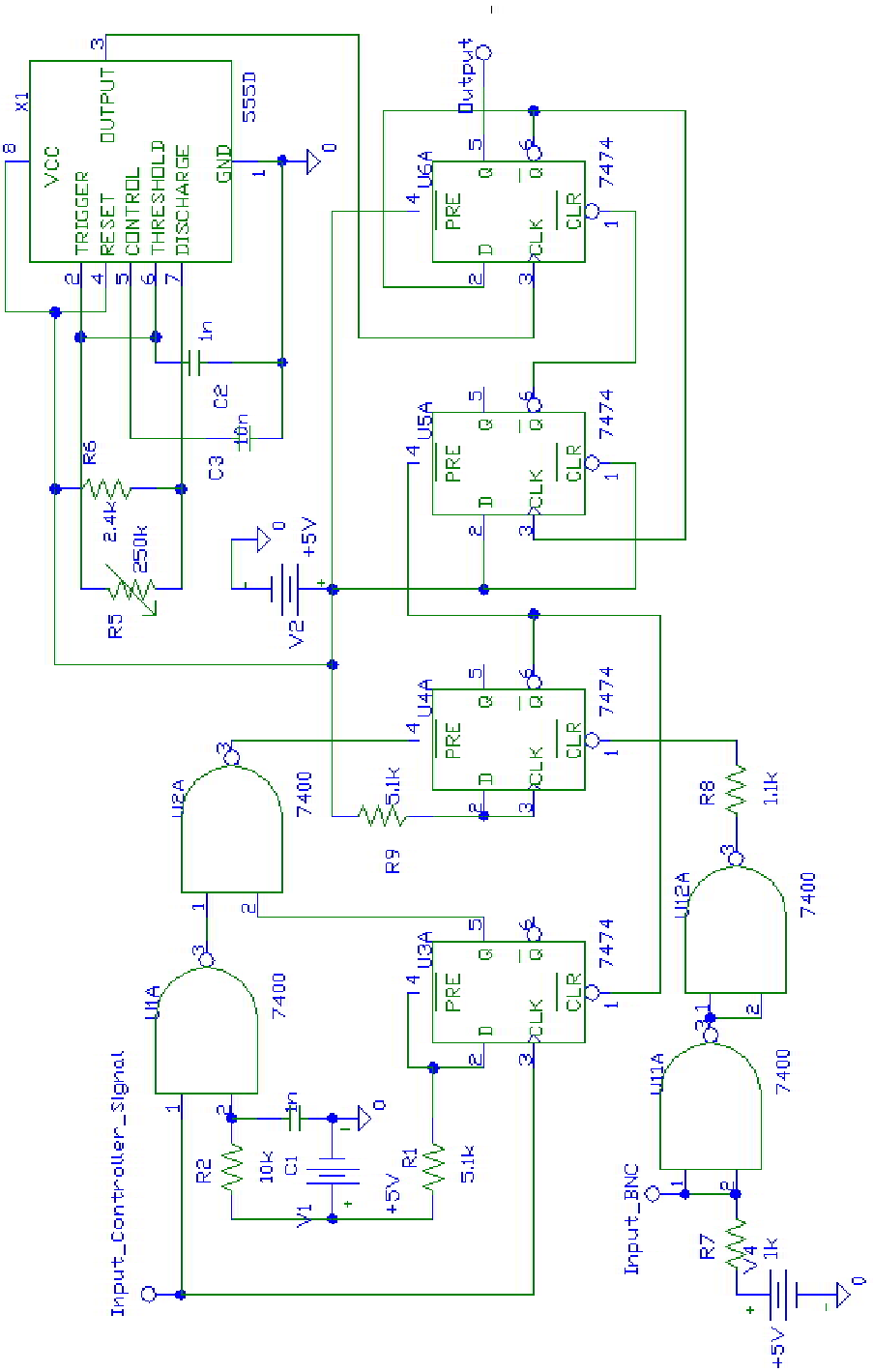

Circuit Schematic 5. Inchworm controller circuit layout

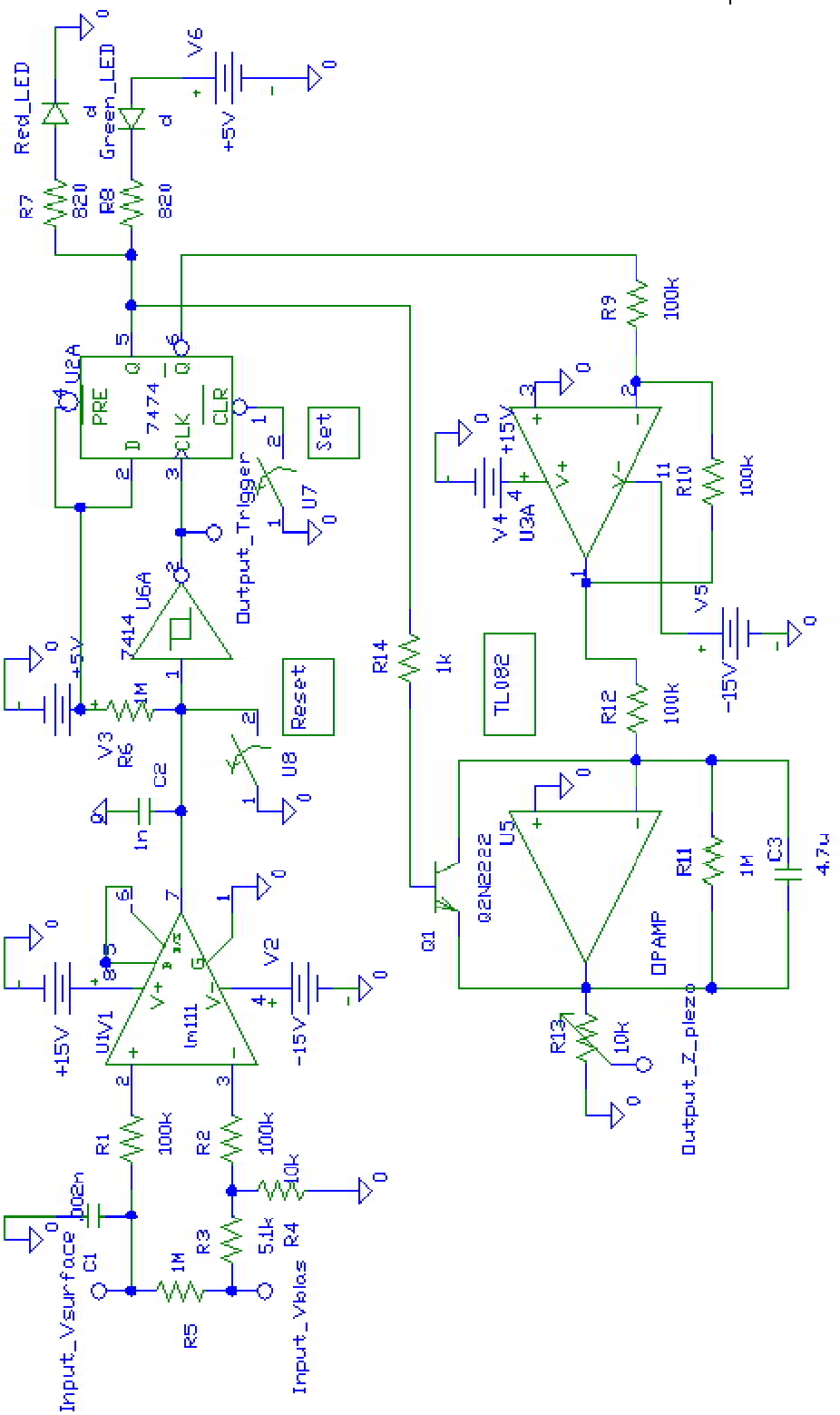

Circuit Schematic 6. NanoEDM controller circuit layout

Appendix C: AutoCAD Drawings

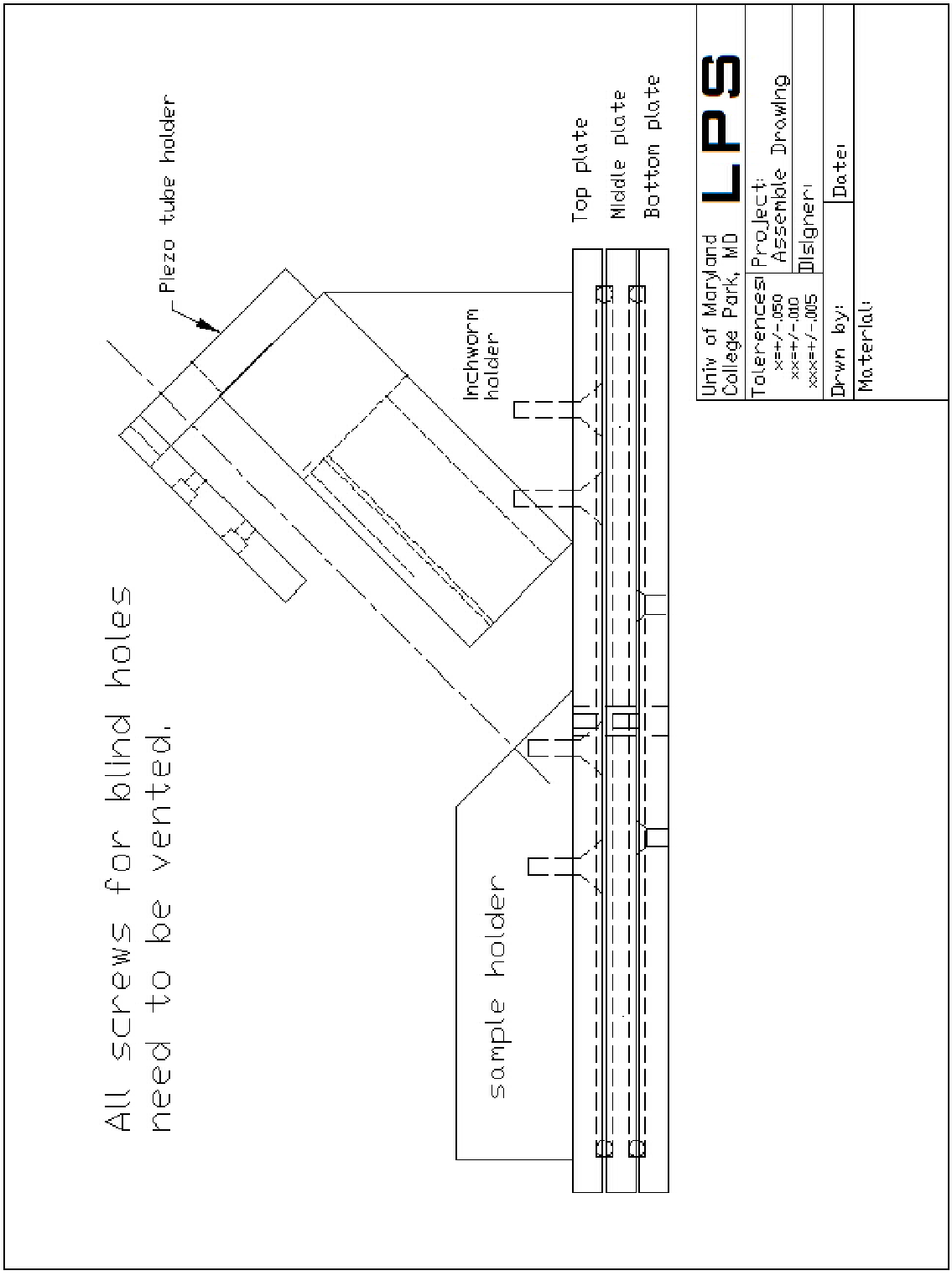

Drawing 1. Assembled Drawing

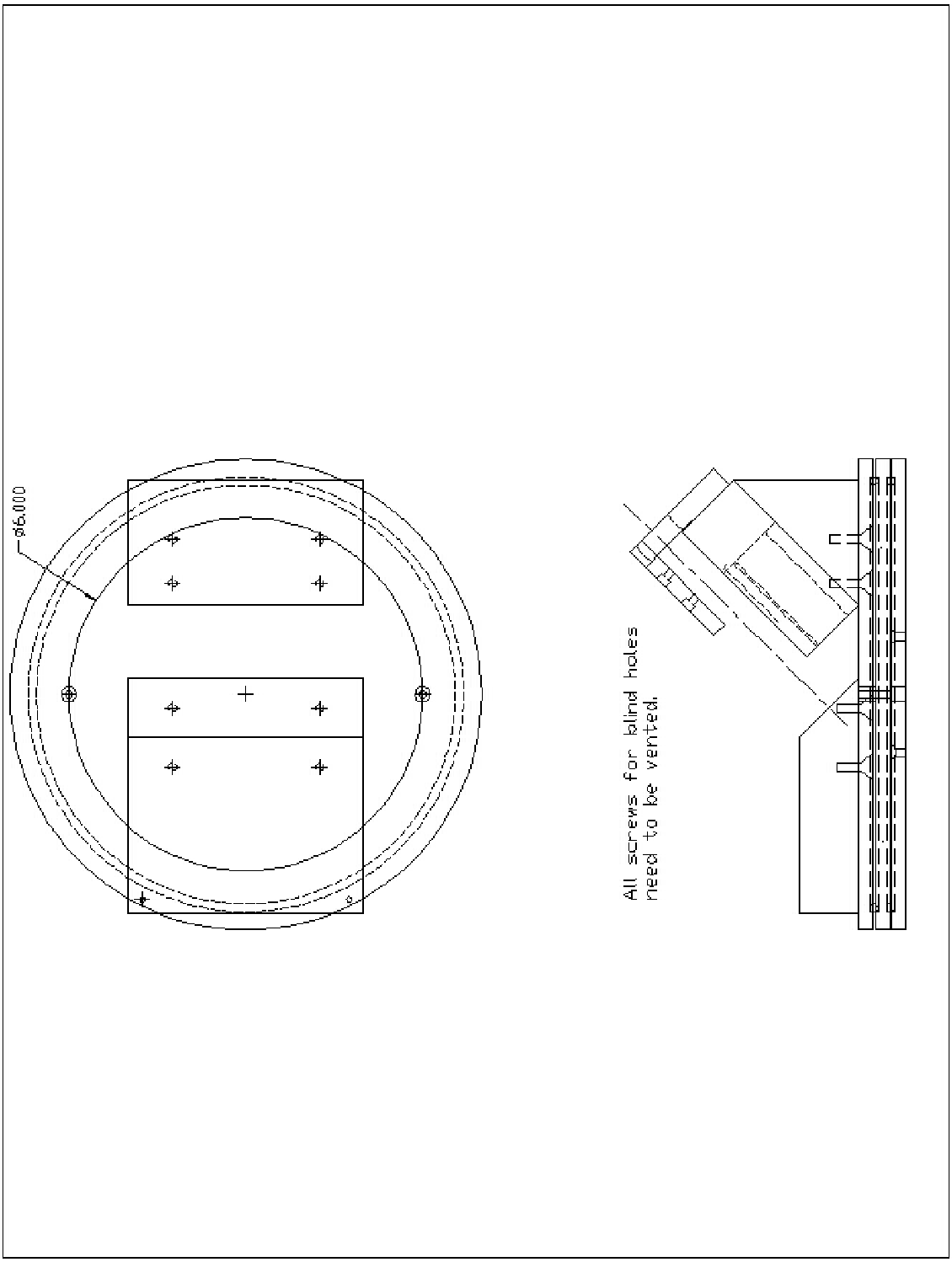

Drawing 2. Assembled Drawing (top view and side view)

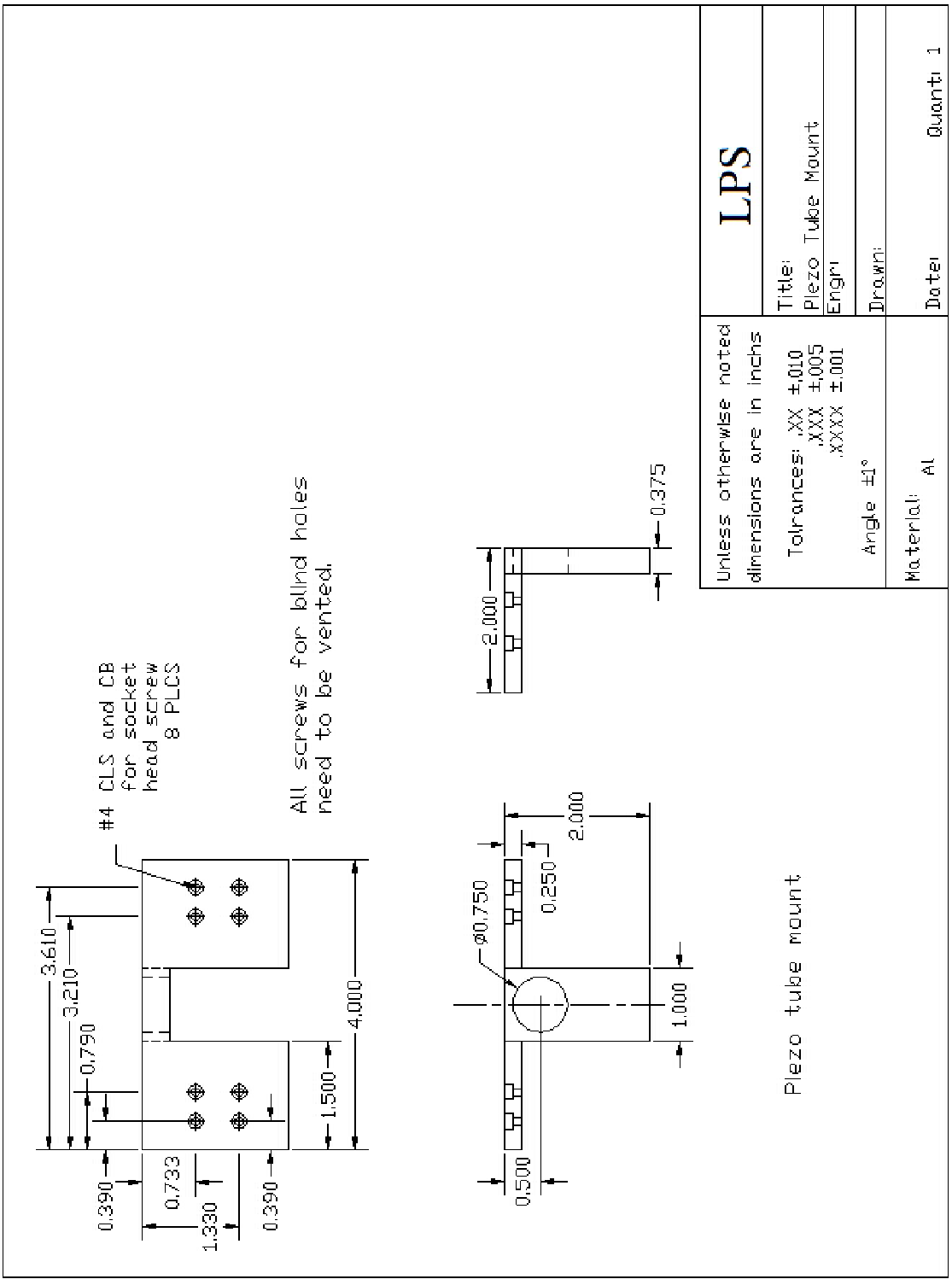

Drawing 3. Piezo Tube Mount

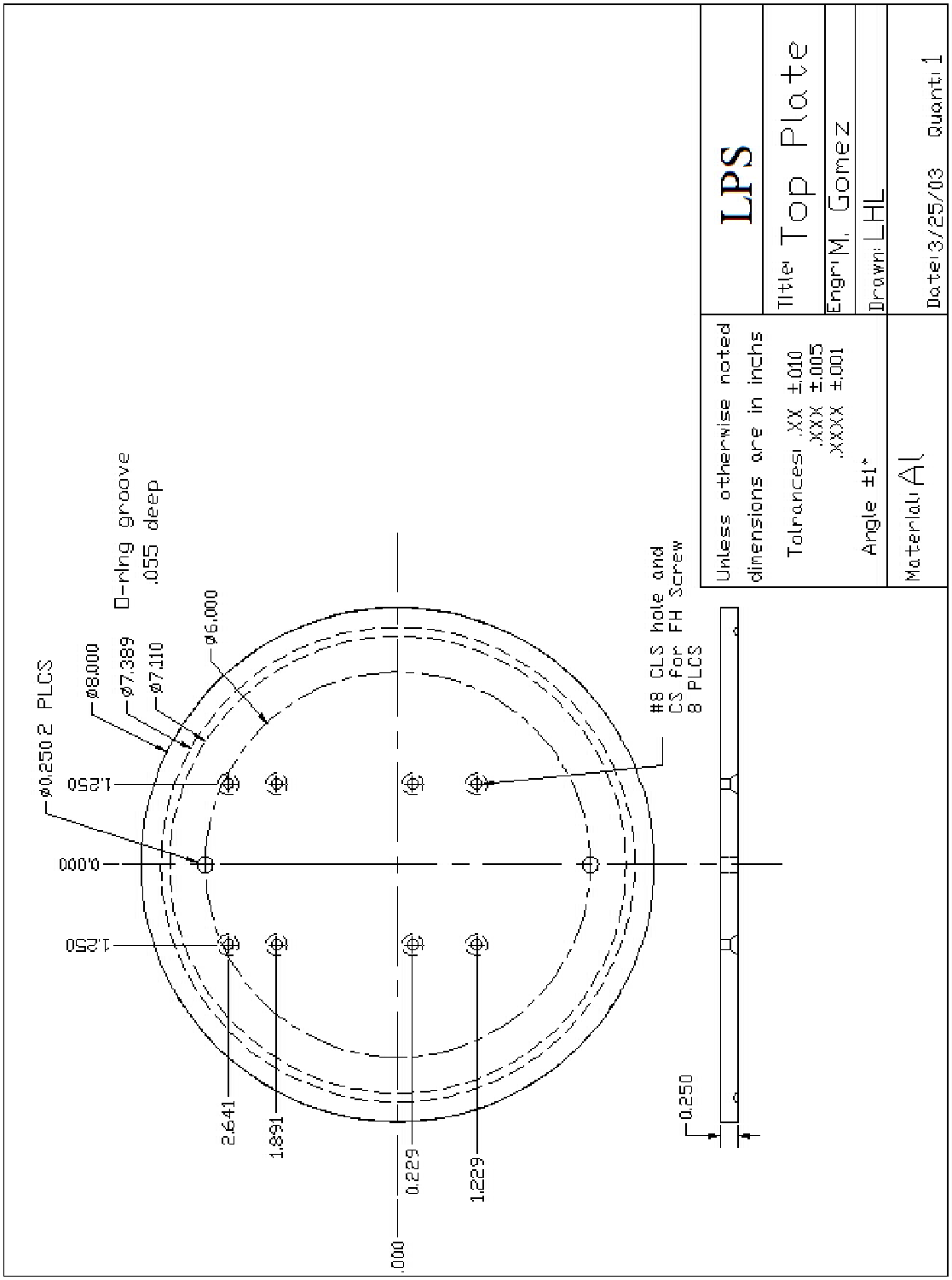

Drawing 4. Top Plate

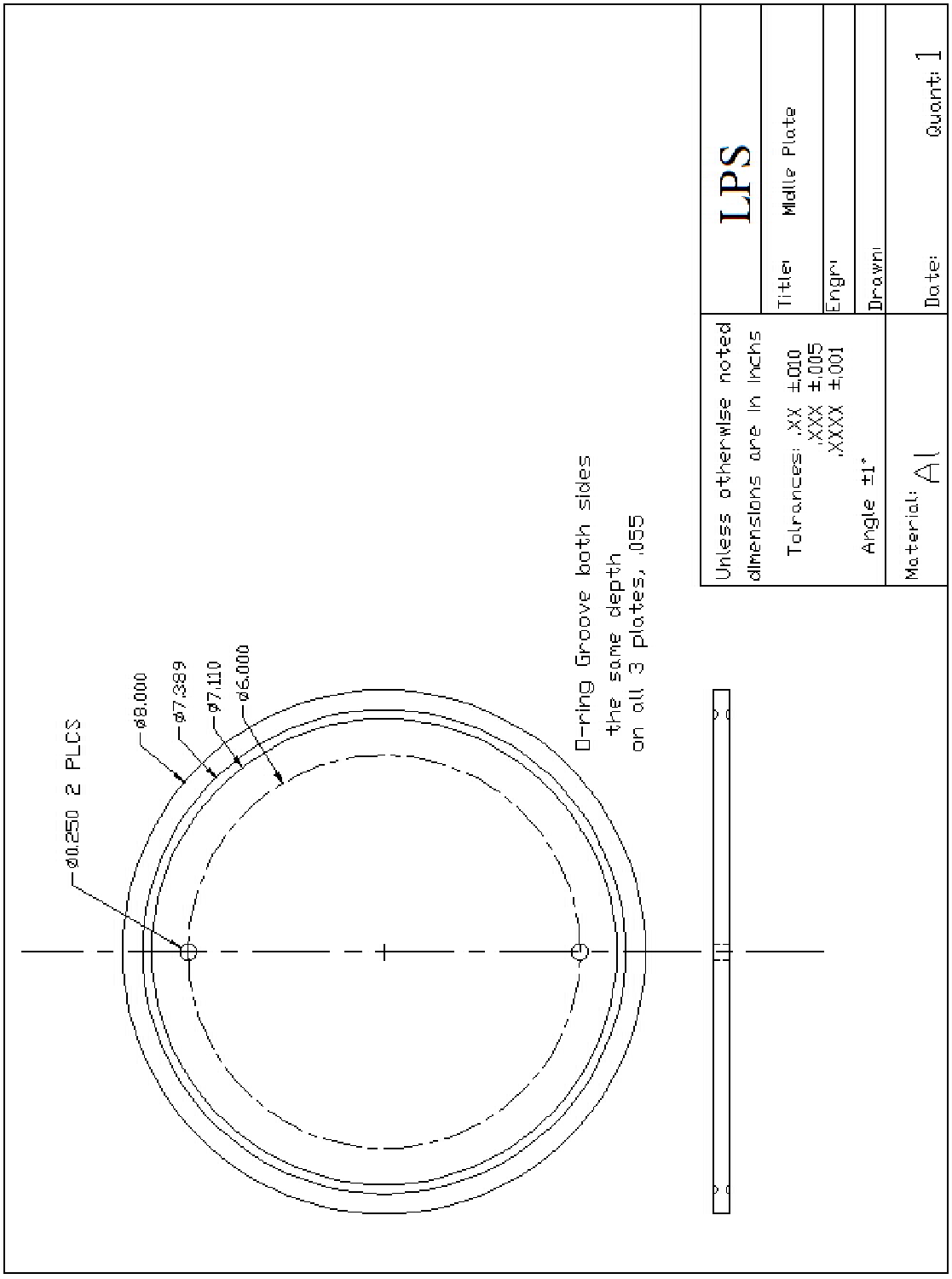

Drawing 5. Middle Plate

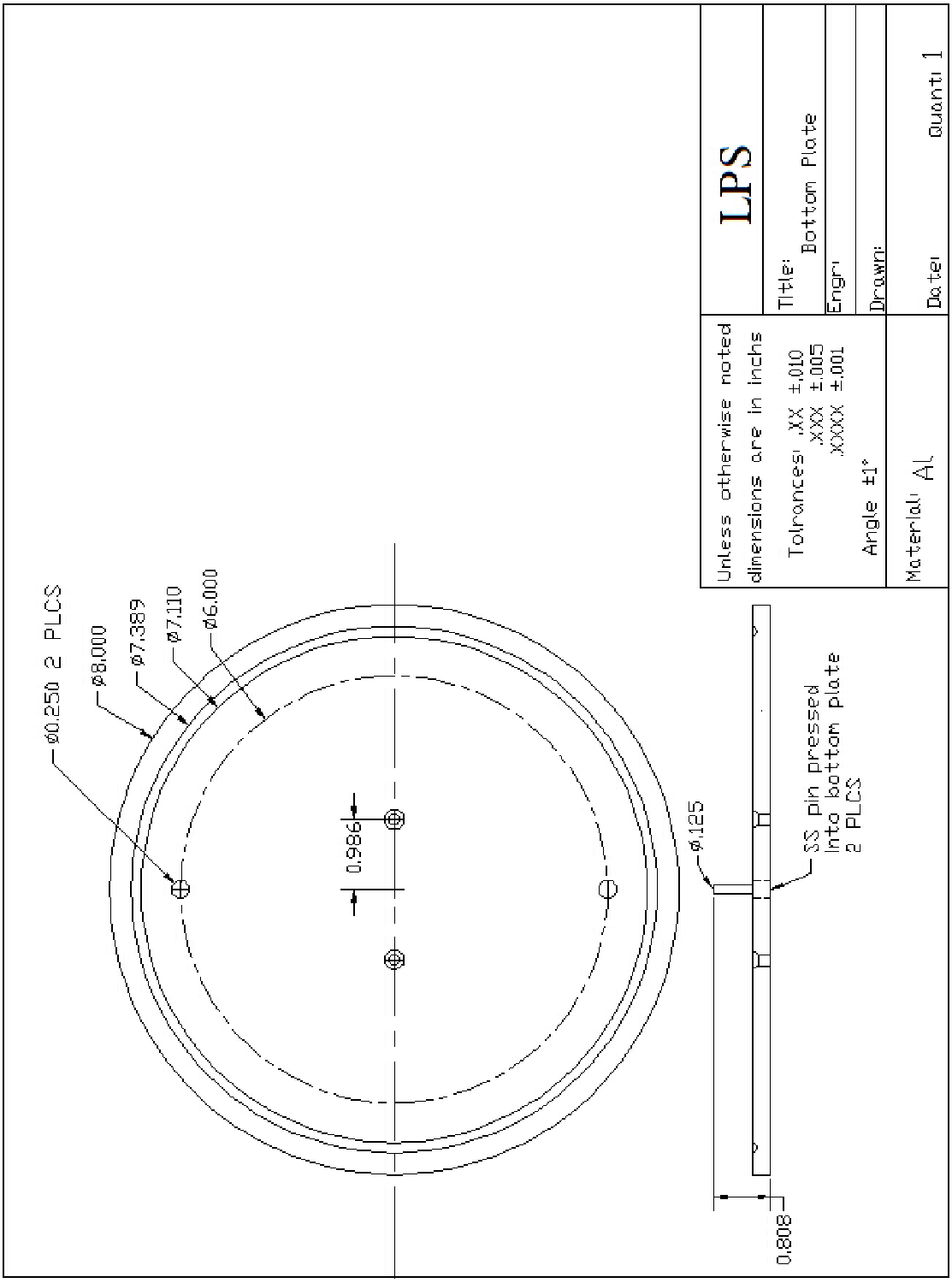

Drawing 6. Bottom Plate

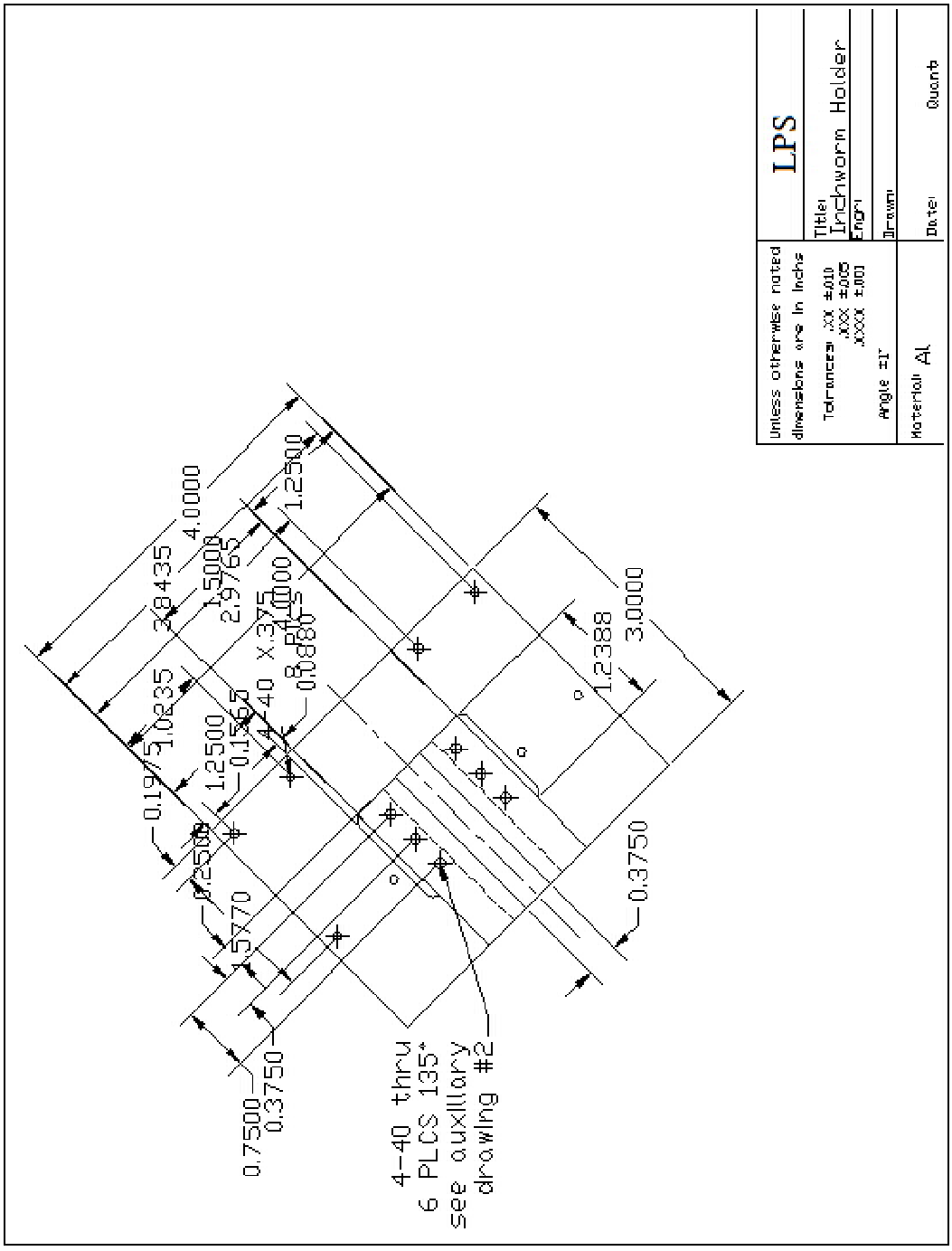

Drawing 7. Inchworm Holder

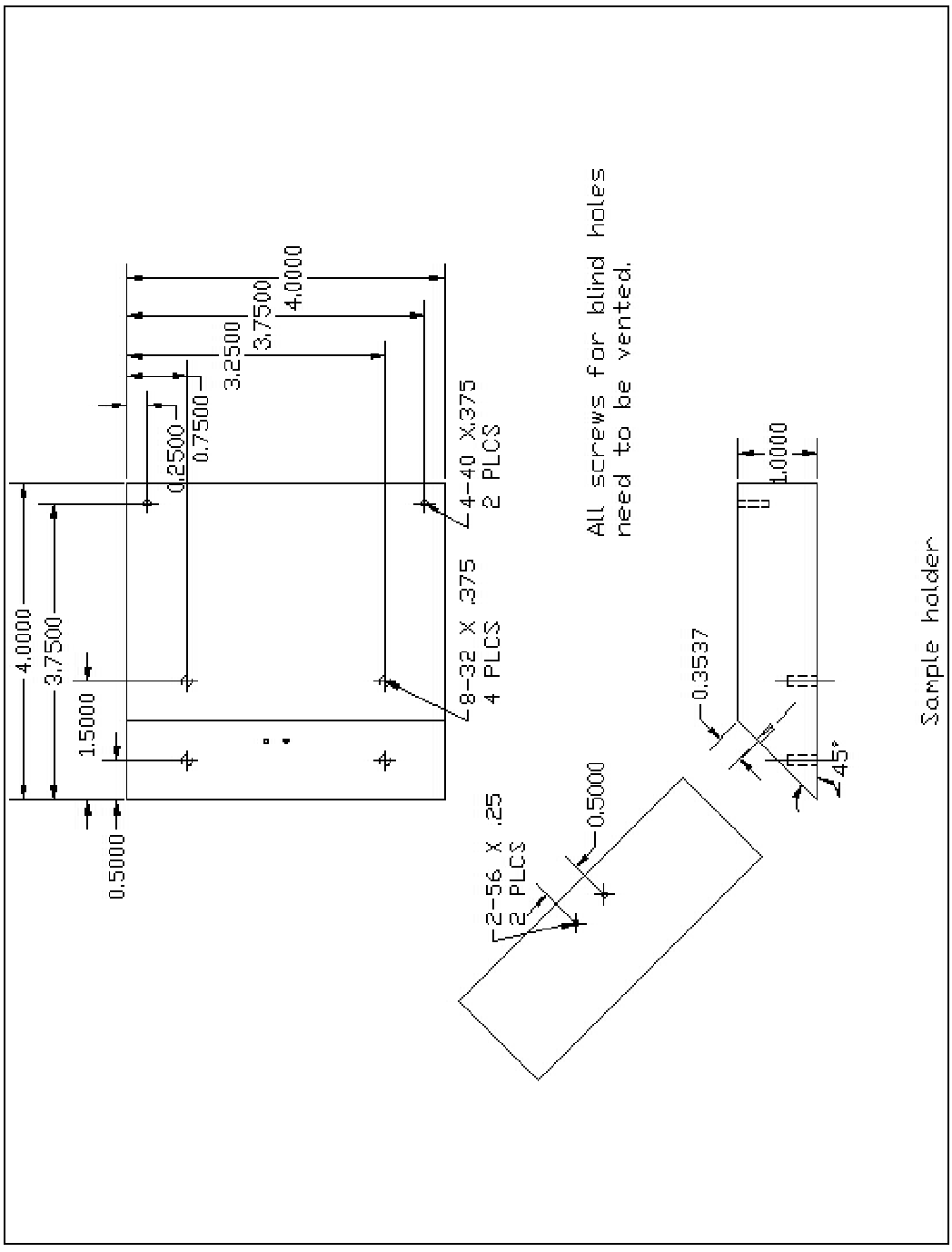

Drawing 8. Sample Holder

Bibliography

1. E.J. Weller, M. Haavisto, *Nontraditional Machining Processes* 2nd edition, Society of Manufacturing Engineers, Dearborn, MI, 1984

2. K.P. Rajurkar, G. Sathyanarayanan, R. Komanduri, *Advances in Non-Traditional Machining* PED-Vol.22, The American Society of Mechanical Engineers, New York, NY, 1986

3. S. Kalpakjian, S.R. Schmid, *Manufacturing Engineering and Technology* 4th edition, Prentice Hall, Upper Saddle, NJ 2001

4. Hugh Jack, *Manufacturing Engineer on a disk: Electric Discharge Machining (EDM)*, http://claymore.engineer.gvsu.edu/~jackh/eod/manufact/manufact-277.html , 2001

5. James Brown, *Advanced Machining Technology Handbook*, McGraw-Hill, New York, NY, 1998

6. D.D. DiBitonto, P.T. Eubank, M.R. Patel, M.A. Barrufet, "Theoretical models of the electric discharge machining process. I. A simple cathode erosion model", *J. Appl. Phys.* 66 (9) pp. 4095-4103 (1989)

7. P.T. Eubank, M.R. Patel, M.A. Barrufet, B. Bozkurt, "Theoretical models of the electric discharge machining process. III. The variable mass, cylindrical plasma model", *J. Appl. Phys.* 73 (11) pp. 7900-7909 (1989)

8. S. Das, M. Klotz, F. Klocke, "EDM simulation: finite element-based calculation of deformation, microstructure and residual stress", *J. Mat. Proc. Tech.* 142 pp. 434-451 (2003)

9. Nobelprize.org, *The 1986 Nobel Prize in Physics*, http://nobelprize.org/physics/laureates/1986/press.html

10. Nobelprize.org, *The Scanning Tunneling Microscope*, http://nobelprize.org/physics/educational/microscopes/scanning/

11. D.A. Bonnell, *Scanning Tunneling Microscopy and Spectroscopy*, VCH Publishers, Inc., New York, NY, 1993

12. Ultra High Vacuum Inchworm Motor Instruction Manual, Burleigh Instruments, Inc., Fishers, NY

13. L. Reimer, *Scanning Electron Microscopy* 2nd edition, Springer-Verlag, Berlin, Germany, 1998